Synchronization of Golgi and Granule Cell Firing in a Detailed Network Model of the Cerebellar Granule Cell Layer

REINOUD MAEX AND ERIK DE SCHUTTER
Born-Bunge Foundation, University of Antwerp, B-2610 Antwerp, Belgium

Maex, Reinoud and Erik De Schutter. Synchronization of Golgi and granule cell firing in a detailed network model of the cerebellar granule cell layer. *J. Neurophysiol.* 80: 2521–2537, 1998. The granular layer of the cerebellum has a disproportionately large number of excitatory (granule cells) versus inhibitory neurons (Golgi cells). Its synaptic organization is also unique with a dense reciprocal innervation between granule and Golgi cells but without synaptic contacts among the neurons of either population. Physiological recordings of granule or Golgi cell activity are scarce, and our current thinking about the way the granular layer functions is based almost exclusively on theoretical considerations. We computed the steady-state activity of a large-scale model of the granular layer of the rat cerebellum. Within a few tens of milliseconds after the start of random mossy fiber input, the populations of Golgi and granule cells became entrained in a single synchronous oscillation, the basic frequency of which ranged from 10 to 40 Hz depending on the average rate of firing in the mossy fiber population. The long parallel fibers ensured, through α-amino-3-hydroxy-5-methyl-4-isoxazolepropionic acid-mediated synapses, a coherent excitation of Golgi cells, while the regular firing of each Golgi cell synchronized all granule cells within its axonal radius through transient activation of their γ-aminobutyric acid-A ($GABA_A$) receptor synapses. Individual granule cells often remained silent during a few successive oscillation cycles so that their average firing rates, which could be quite variable, reflected the average activities of their mossy fiber afferents. The synchronous, rhythmic firing pattern was robust over a broad range of biologically realistic parameter values and to parameter randomization. Three conditions, however, made the oscillations more transient and could desynchronize the entire network in the end: a very low mossy fiber activity, a very dominant excitation of Golgi cells through mossy fiber synapses (rather than through parallel fiber synapses), and a tonic activation of granule cell $GABA_A$ receptors (with an almost complete absence of synaptically induced inhibitory postsynaptic currents). These three conditions were associated with a reduction in the parallel fiber activity, and synchrony could be restored by increasing the mossy fiber firing rate. The model predicts that, under conditions of strong mossy fiber input to the cerebellum, Golgi cells do not only control the strength of parallel fiber activity but also the timing of the individual spikes. Provided that their parallel fiber synapses constitute an important source of excitation, Golgi cells fire rhythmically and synchronized with granule cells over large distances along the parallel fiber axis. According to the model, the granular layer of the cerebellum is desynchronized when the mossy fiber firing rate is low.

INTRODUCTION

A knowledge of the firing pattern of parallel fibers (PFs) is essential to any theory of the function of the cerebellar cortex. Because the only output neurons, the Purkinje cells, receive synapses from ~200,000 PFs (Harvey and Napper 1991), activity in a single PF is unlikely to be effective, whereas massive PF activity would abolish response selectivity. It therefore has been proposed (Marr 1969) that a Purkinje cell should be regarded as an output element of several functional circuits, each activating ≥500 PF synapses. The activation of too many PFs, on the other hand, would be prevented by the suppressive action that the inhibitory Golgi cells exert on granule cells. According to this widely accepted theory, ''the role of the Golgi cell would be to reset the threshold of the granule cell according to the conditions of the input'' (Palay and Chan-Palay 1974).

In the present paper, we examine the function of Golgi cells in granular layer activity. The connectivity of cerebellar Golgi and granule cells is summarized in Fig. 1*A*. A few modeling studies of this circuitry have tried to support the gain control (or threshold setting) function of Golgi cells, but they either used logical units (Moore et al. 1989; Pellionisz and Szentágothai 1973) or linear units (Chauvet 1995) as simplified model neurons, or they simulated the effect of inhibition on only a single model granule cell (Gabbiani et al. 1994). Like inhibitory neurons in other systems, however, a Golgi cell could be expected to control not only the firing threshold or firing rate of its efferent granule cells but also the exact timing of their action potentials (Cobb et al. 1995; Lytton and Sejnowski 1991).

The compact organization of granule cells and parallel fibers within the cerebellar cortex has prevented experimental measurements of their in vivo activity until now. We therefore have simulated a network of compartmental neurons representing the in vivo rat granular layer, starting from the in vitro dynamics of the component neurons and synapses and from the detailed connection pattern as it has emerged from anatomic observations (Palay and Chan-Palay 1974) and from electrical stimulation experiments (Eccles et al. 1967). In this initial study, the model mossy fibers fired randomly at a constant average rate. This allowed the granular layer to evolve toward a steady state, which was easier to describe quantitatively and hence was most appropriate for parameter analysis.

As we partly reported in abstract form (Maex et al. 1996), the feedback inhibition exerted by Golgi cells on granule cells caused the model granular layer to fire rhythmically and synchronized. Recently, two experimental studies have revealed prominent oscillations in the field potentials recorded from the granular layer of behaving rats (Hartmann and Bower 1998) and monkeys (Pellerin and Lamarre 1997). We therefore analyzed extensively the conditions for the emergence of oscillations in the granular layer model.

0022-3077/98 $5.00

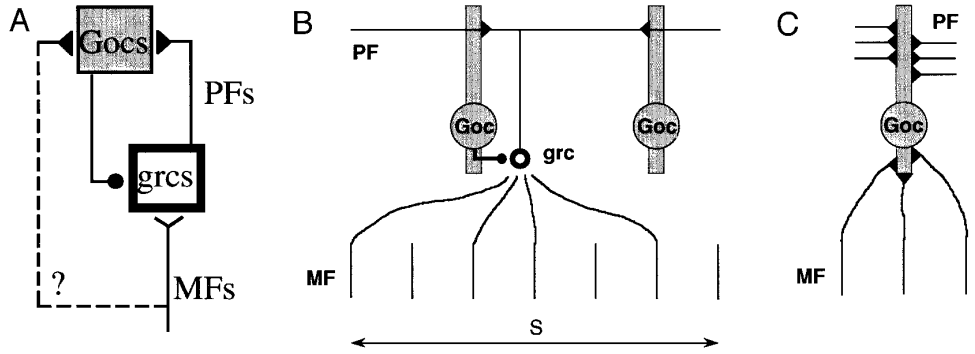

FIG. 1. Granular layer model comprises mossy fibers (MFs), granule cells (grcs), and Golgi cells (Gocs). MFs and grcs make excitatory synapses, Gocs are inhibitory. *A*: lumped circuit diagram. Inhibition to grcs can follow 2 pathways: feedforward (MF → Goc → grc) or feedback (MF → grc → Goc → grc). Actual contribution of monosynaptic MF input to Goc excitation is not known; this branch is therefore marked with a ''?''. *B*: topography of the connections and synaptic input to grcs. The 30 Gocs, 2 of which are shown, are evenly positioned at 300 μm intervals along a 9-mm array, together with a variable number of MFs and grcs. For clarity, the synaptic inputs to only a single grc are shown. The grc receives excitation from 4 MFs which may not span a distance larger than *S*, which was equal to 6 inter-MF intervals in this figure (↔). The grc also receives inhibition from the closest Goc. The grc axon forms a 5 mm long parallel fiber (PF), which makes excitatory synapses on the apical dendrites of the schematically drawn Gocs. *C*: synaptic input to Gocs. In addition to parallel fiber excitation, each Goc also receives excitation from a contiguous set of MFs the synapses of which are drawn schematically on the basal dendrite. Note, however, that the simulated Gocs were single compartmental. Monosynaptic MF excitation of Gocs was switched off in the standard model. See METHODS for more details.

METHODS

We first present the network model and develop thereafter, in more detail, the models of the component neurons and synapses. It will be demonstrated that the isolated model granule and Golgi cells, although constructed from incomplete data, faithfully reproduced the actual responses recorded from these neurons in slice preparations. At the end, the tools for the analysis of the network responses are described.

Network dimensions and connectivity

The model was a network of mossy fibers (MFs), granule cells (grcs), and Golgi cells (Gocs), originally conceived as a two-dimensional (2D) grid in the plane of the parallel fiber (PF) and sagittal axes. However, one-dimensional (1D) networks extending along the PF axis only and representing a ''beam'' of granular layer (Eccles et al. 1966) were found to display the same dynamics as 2D grids and allowed us, in addition, to simulate more realistic neuronal and synaptic densities. We therefore present in this article results computed on a 1D beam of 9 mm length. This length was determined by the need to reduce border effects around a central area longer than a single PF.

Along this beam, a fixed number of 30 Gocs were aligned at 300-μm intervals (Palkovits et al. 1971) (Fig. 1*B*). For every Goc, it was estimated that there are ~1,000 grcs in the rat cerebellum based on a grc/Purkinje cell ratio of 274 (Harvey and Napper 1991) and a Purkinje/Goc ratio of 3.22 (Palkovits et al. 1971), but it was impractical to always simulate 30,000 grcs. Instead their number was reduced, and networks with varying numbers of grcs were compared. A maximum variability in grc responses within such reduced networks was preserved, however, by assigning each model grc a unique set of four different MF afferents.

To accomplish this, a number N_{mf} of MFs were evenly distributed along the Goc array first. Along this array, a parameter *S* (Fig. 1*B*) defined the maximum distance allowed between two MF afferents to a single grc. This spatial span *S* can be considered a measure of the divergence of MFs by ramification in the granular layer (Palay and Chan-Palay 1974). A unique grc was then created for every combination of four different MFs spanning a distance $\leq S$. This was achieved by passing from left to right along the MF array and combining each successive MF with all possible triplets from the subarray of *S* MFs at its left-hand side. As a consequence, when *S* is expressed in units of inter-mossy-fiber distance, the total number of grcs N_{gc} was approximately

$$N_{gc} \approx N_{mf} \frac{S(S-1)(S-2)}{6} \quad (1)$$

For example, a circuit with 540 MFs counted 537 grcs for $S = 3$ and 10,695 grcs for $S = 6$. Note also that with this MF-to-grc innervation pattern, the population of grcs functioned as a combinatorial expander of the population of MFs, as proposed by Marr (1969) and Albus (1971).

Each grc was placed at the center of its set of MF afferents (Fig. 1*B*). From the above, a grc received, through α-amino-3-hydroxy-5-methyl-4-isoxazolepropionic acid (AMPA)- and *N*-methyl-D-aspartate (NMDA)-receptor channels, excitation from four different MFs within a radius of *S/2*. In addition a grc received, through a γ-aminobutyric acid-A ($GABA_A$) channel, inhibition from the closest Goc.

The grc axon, which was not explicitly modeled, ran in each of two opposite directions over a distance of 2.5 mm (PF length of 5 mm) (Mugnaini 1983; Pichitpornchai et al. 1994) and allowed the grc to make a PF synapse on each of the at most 17 intervening Gocs with a chosen probability *P*. The delays of these grc-to-Goc PF synapses were set to the ratios of the intersomatic distances over the PF conduction speed (0.5 m/s), and hence measured 0–5 ms. Gocs also could receive monosynaptic excitation from a set of MFs (Fig. 1*C*). The PF and MF synapses on Gocs had AMPA receptor channels (Dieudonné and Kehoe 1996; Midtgaard 1992).

Model granule cells

Our starting point was a model of an in vitro turtle grc (Gabbiani et al. 1994). This model was first modified to represent a rat grc in vivo and next simplified to reduce the computational load imposed by the large grc population. The complete equations can be found in the APPENDIX.

SINGLE-COMPARTMENTAL REDUCTION TO RAT DIMENSIONS. The 13 dendritic and somatic compartments were lumped into a single, isopotential spherical soma. This is justified because rat

grcs have been reported to be electrically very compact (Bardoni and Belluzzi 1993; D'Angelo et al. 1995; Silver et al. 1992). A virtual soma diameter of 10 μm produced a model cell capacitance of 3.14 pF, which is a typical value for rat grcs (Barbour 1993; Bardoni and Belluzzi 1993; Cull-Candy et al. 1989; D'Angelo et al. 1995; Kaneda et al. 1995; Silver et al. 1992). Note that the diameter was larger than the 6 μm of actual grcs (Palay and Chan-Palay 1974) but needed to compensate for the membrane surface area of the missing dendrites.

IN VIVO KINETICS. Assuming temperature-dependent kinetics with a Q_{10} factor of 3, all rate constants describing the voltage-gated channels at room temperature were multiplied by 5 (De Schutter and Bower 1994a). Because this change in time scale decreased the amount of charge transferred through these channels, which consequently disturbed the dynamics of the neuron as a whole (Rinzel and Ermentrout 1989), the channels' densities or peak conductances needed to be increased as well, mostly by a factor of 2 (Q_{10} for diffusion of 1.2–1.5) (Hille 1992). The resulting peak conductances were: inactivating Na^+ channel (NaF) 172 nS, high-voltage-activated Ca^{2+} channel (CaL) 2.9 nS, delayed rectifier (Kdr) 28 nS, A-type K^+ channel (KA) 3.6 nS, Ca^{2+}-dependent K^+ channel (KC) 56.5 nS, and anomalous inward rectifier (H) 97.1 pS. Similarly, we adapted all synaptic conductances to have an acceleration of 3 between room temperature and 37°C (Q_{10} factor of 2) (Otis and Mody 1992; Silver et al. 1996), resulting in the following time constants: AMPA receptor channels rise 0.03 ms, decay 0.5 ms (Silver et al. 1992); NMDA channels rise 1 ms, decay 13.3 ms (Gabbiani et al. 1994); and $GABA_A$ channels rise 0.31 ms, decay 8.8 ms.

EXCITABILITY. Rat grcs have a much higher firing threshold than turtle grcs, reaching >20 mV (D'Angelo et al. 1995). This was achieved by shifting all voltage-dependent functions, including the one describing the Mg^{2+} block of the NMDA channels (Gabbiani et al. 1994), 10 mV toward more positive voltages. The A-type potassium current was based on voltage-clamp data from rat grcs (Bardoni and Belluzzi 1993). The reversal potential of the leak current was distributed uniformly between −70 and −60 mV among the model grcs, resulting in a realistic resting potential distribution between −64.6 and −60.6 mV (D'Angelo et al. 1995; Puia et al. 1994). Finally, the peak ionic conductances induced by the activation of AMPA and NMDA receptor channels at a single MF synapse were calibrated after recent current-clamp data (D'Angelo et al. 1995) and voltage-clamp data (Silver et al. 1996). A single MF activated a grc AMPA channel with a peak conductance of 647 pS; the peak conductance of the NMDA channel was voltage dependent with an asymptotic value of 748 pS.

Responses of a model granule cell

Figure 2 illustrates how a model grc constructed as described above generated typical responses to current injection (*A*) and to synaptic stimulation (*B* and *C*).

ELECTRICAL STIMULATION. Application of 5 pA outward current hyperpolarized the grc from its resting potential of −62.6 up to −89.1 mV, which corresponded to an input resistance of 5.3 GΩ (*A*, bold curve). This high value is typical of rat cerebellar grcs in slice recordings (D'Angelo et al. 1995; Kaneda et al. 1995; Puia et al. 1994; Silver et al. 1992, 1996). During the application of inward current (A, thin curve), the grc fired regularly and without adaptation, with a threshold of 5–6 pA and a mean slope of the frequency versus intensity curve of 5 Hz/pA, which both are average values of slice grcs (Brickley et al. 1996; D'Angelo et al. 1995).

SYNAPTIC STIMULATION. The membrane potential responses to activation of increasing numbers of MFs are shown in Fig. 2*B*. Activation of a single MF evoked a subthreshold excitatory post-

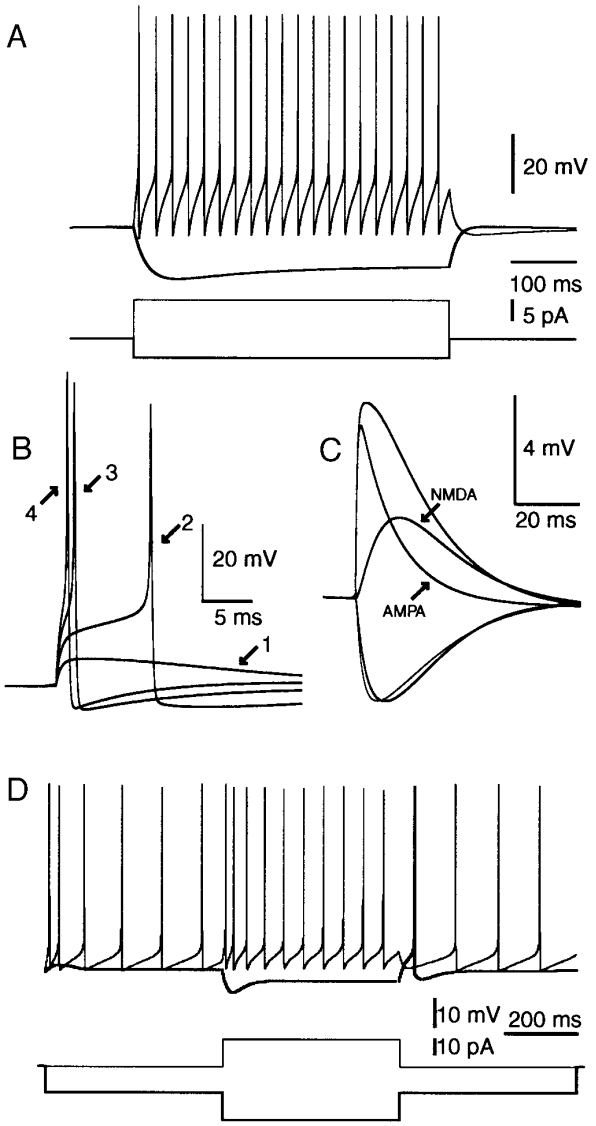

FIG. 2. Model grcs (*A*–*C*) and Gocs (*D*) react to current injection (*A* and *D*) and synaptic stimulation (*B* and *C*) like actual neurons in slice. *A*: responses of a model grc to the 500-ms application of 10-pA inward current (thin trace) and 5-pA outward current (bold trace). *B*: responses of a model grc to the synchronous activation of the synapses from 1, 2, 3, and 4 MFs (as marked). *C*: responses of a model grc to the activation of a single MF synapse (upward traces) and of a Goc synapse (downward traces). Excitatory postsynaptic potential has been dissected into its 2 components, evoked by the selective activation of the α-amino-3-hydroxy-5-methyl-4-isoxazolepropionic acid (AMPA)- and the *N*-methyl-D-aspartate (NMDA)-receptor channel, respectively. For the inhibitory postsynaptic potential, the peak conductance of the γ-aminobutyric acid-A ($GABA_A$) receptor channel measured 600 pS in this figure. Standard inhibitory postsynaptic potential (bold trace) is compared with the response produced when the underlying conductance was modeled by a biexponential decay function (thin curve: time constants of 7 and 36 ms at room temperature and with a 33% contribution of the slow component). *D*: responses of a model Goc, which fired spontaneously at a rate of 8.6 Hz, to hyper- and depolarizing current injection. Thin trace, response when 20 pA inward current was applied during 500 ms. Bold trace, response during the transition from 20 to 40 pA and back to 20 pA outward current, applied in 500-ms steps.

synaptic potential (EPSP) of 7.3 mV after 3 ms. To cross the firing threshold, two or three MFs had to be activated simultaneously (depending on the resting membrane potential of the model grc), as in slice grcs (D'Angelo et al. 1995). The response to activation

of a single MF has been magnified in Fig. 2*C* and is compared with the response evoked when the NMDA receptor channel had been blocked completely (curve labeled AMPA). It can be seen that the current through the AMPA channel accounted for 89% of the potential peak and that it carried 44% of the charge into the cell. The time course of the response to synaptic inhibition is also shown in Fig. 2*C* (bold curve) and almost completely overlapped the response produced with an inhibitory conductance that decayed after a biexponential function (thin curve), which is the type of function most frequently used to describe experimental data on grc inhibition (Brickley et al. 1996; Kaneda et al. 1995; Puia et al. 1994). The actual strength in vivo of the inhibitory synapses is not known. For a peak conductance of 600 pS (Brickley et al. 1996), the inhibitory postsynaptic potential (IPSP) measured −3.8 mV after 9 ms.

Model Golgi cells

Because of a lack of morphological reconstructions of Goc dendrites, Gocs were modeled as single spherical compartments too. A virtual diameter of 30 μm yielded a total cell capacitance of 28 pF (Dieudonné 1995). Similarly, because insufficient voltage-clamp data were available, Gocs were, as a first approximation, modeled with the same set of channels as used for the grc model but without the 10 mV shift of the rate constant functions. From this, spontaneous activity was introduced by using a less negative reversal potential for the leak current, which was distributed uniformly between −60 and −50 mV. The resulting spontaneous firing rates (6.6–10.9 spikes/s, mean 8.8) were comparable to those recorded in vitro in turtles (13 spikes/s) (Midtgaard 1992) and rats (3–5 spikes/s) (Dieudonné and Kehoe 1996). The peak conductances of the voltage-gated channels thereafter were tuned to allow for a qualitative reproduction of the current-clamp traces recorded from turtle Gocs (Midtgaard 1992), resulting in the following values: NaF, 1,131 nS; CaL, 23.5 nS; Kdr, 192 nS; KA, 14.8 nS; KC, 16.2 nS; and H, 4.85 nS. With this particular parameter set, the model Goc reproduced recently reported responses of rat Gocs (Dieudonné 1998).

Finally, the Gocs were provided with AMPA receptor channels for their MF and PF synapses (Dieudonné 1995; Midtgaard 1992). The same synaptic channel kinetics were used as for grcs. The global peak conductance (see further) of the PF-activated AMPA channel of Gocs was put at 45.5 nS. This value allowed for a maximal global synaptic charge transfer of ~1 pC, which corresponds well with the 2 pC recently estimated to be needed to reach threshold from −75 mV in slice Gocs (Dieudonné 1998).

Responses of a model Golgi cell

ELECTRICAL STIMULATION. Figure 2*D* illustrates the typical responses of a model Goc to current injection. The input resistance was measured by suppressing all spontaneous activity with a −20-pA current and simulating the response to an additional −20-pA current step (thick curve). The model Goc hyperpolarized hereupon from −64.1 up to −72.7 mV, corresponding to an input resistance of 428 MΩ. On return to the −20-pA current level, the Goc fired a spike on top of a rebound depolarization. This rebound depolarization and the sag in the hyperpolarization plateau were elicited by the large, anomalously activated H current. Interestingly, an H current recently has been postulated to cause rebound spikes in rat Gocs (Dieudonné 1998). When a 20-pA depolarizing current was applied (thin curve), the model Goc adapted its increased firing rate because of the slow activation of its Ca^{2+}-dependent K^+ channel. A similar adaptation has been reported in rat Gocs (Dieudonné 1998). Withdrawal of the stimulus caused a slowly decaying hyperpolarization.

SYNAPTIC STIMULATION. The PF- and MF-induced EPSPs had the same time courses as the AMPA-mediated component of a grc EPSP, which was shown in Fig. 2*C*. Their amplitudes were varied extensively between simulations (see Figs. 4 and 5).

Mossy fibers

Finally, each mossy fiber was modeled as a binary variable signaling the arrival of a spike that synchronously activated all grcs and Gocs to which the MF was connected synaptically. The probability of ''firing'' of a model MF was independent of its own firing history and of that of any other MF, except for a 5-ms refractory period after each spike. This Poisson distribution of the instantaneous MF firing rates reflected our ignorance of the fine structure present in and between the spike trains conveyed by actual MFs in a behaving rat. Only a tonic pattern of MF input was used, usually 10 s in duration, because this allowed us to study the dynamics of the granular layer under steady-state conditions. In most simulations, all MFs fired at the same average rate of 40 spikes/s.

Synaptic weights, normalization, and randomization

Because each model neuron was isopotential and because model synapses had uniform time courses, all synapses originating from afferents belonging to a common population of neurons (or fibers) converged onto a single ''channel'' of the postsynaptic neuron. Hence each model grc was provided with one AMPA, one NMDA, and one $GABA_A$ receptor channel, whereas each Goc had two (PF vs. MF activated) AMPA channels. The maximum conductances of these channels, which will be called ''global peak conductances,'' express the conductance peaks resulting from the simultaneous activation of all their synapses.

To preserve synaptic specificity, each synaptic connection was assigned an individual weight factor (≤ 1) and an individual delay. The peak of the synaptic conductance induced by the arrival of a spike was calculated as the product of the global peak conductance of the postsynaptic channel and the weight factor of that connection. Multiple synaptic connections made by one neuron onto the same postsynaptic neuron were represented as one connection with a single delay and a single weight factor. For example, if a grc had only one Goc afferent, then the global peak conductance of its $GABA_A$ channel should be regarded to represent the cumulative strength of 10 virtual synapses, which is the average number of inhibitory synapses onto grcs (Jakab and Hámori 1988).

All synapses to a postsynaptic channel initially were assigned the same weight factor equal to the inverse of the number of afferents. This normalization guaranteed that a channel's global peak conductance was constant throughout the neurons of a population, even when the numbers of afferents varied as was usually the case for the number of PF afferents to Gocs. This allowed for a fair comparison among the responses of different neurons within a population and, similarly, among the population responses obtained from networks with different synaptic densities (connection probabilities). This strategy also avoided too strong boundary effects at the edges of the circuit. It can be compared with the experimentally observed adaptation of channel densities to the average cell activity (Turrigiano et al. 1998).

After this normalization procedure, pre- and postsynaptic variability was introduced by an independent randomization of the channels' global peak conductances, and of the individual weights and delays of all their afferents. Both were distributed uniformly in a ±15% interval around the mean value. As a consequence of this combined pre- and postsynaptic randomization, the peaks of the conductances of the individual synapses formed a skewed distribution in a [−27.75%, +32.25%] interval around the median.

Finally, synaptic failure and synaptic plasticity were not modeled.

Model versions and parameter settings

The parameters explored in most detail were: the sizes of the populations of MFs and grcs, the densities of innervation between MFs, grcs and Gocs, and the global peak conductances of the corresponding postsynaptic channels.

We describe in RESULTS three versions of the model as follows:

1. The *standard or feedback-inhibition model*: In this model, MFs did not innervate Gocs, hence grc inhibition was always feedback at the population level (Fig. 1, *A* and *B*). This model was most appropriate to elucidate the mechanism underlying the network oscillations and to reveal its most critical parameters. Unless otherwise stated, the standard network comprised 540 MFs, 5,355 grcs, and an average number of 602 PF synapses on each Goc (range: 572–631, connection probability $P = 0.2$). The global peak conductance of the $GABA_A$ receptor channel of a grc was 14.1 nS (or 1.41 nS for each of 10 virtual Goc synapses) and a grc was innervated by its closest Goc only.

2. The *feedforward-inhibition model*: In this model, Gocs also received monosynaptic MF excitation. Hence, grcs received both feedforward and feedback inhibition at the population level (Fig. 1, *A* and *C*). This model probably reflected more physiological conditions but, as a problem, no exact values exist describing the actual contributions of MFs and PFs to Goc excitation in vivo. Compared with the previous model, the global peak conductance of the $GABA_A$ channel of grcs was reduced to 2.4 nS, and each grc was innervated by its four closest Gocs (hence 0.6 nS per afferent Goc).

3. The *tonic-inhibition model*: The synapses from Gocs to grcs had the same parameter values as in the previous model. However, grcs had in addition a tonic GABA channel, which had a very slow decay time constant of 300 ms and was activated by the spikes from all 30 Gocs in the network. This model was used to simulate recent experiments on slices of adult rats, during which a tonic inhibitory current was observed in grcs (Brickley et al. 1996; Wall and Usowicz 1997).

Simulation tools

The models have been constructed and numerically solved with GENESIS 2.1 (Bower and Beeman 1995). More specifically, the sets of differential equations were integrated with a Crank-Nicholson method using a fixed step size of 20 μs. A dedicated Sun UltraSparc computer needed ~18 h processing time to simulate 10-s network time in the standard model. The GENESIS 2.1 scripts used to generate the different versions of the network can be obtained at the URL: http://bbf-www.uia.ac.be/CEREBELLUM/network.html.

Data analysis

In first instance, the average firing rates of the grc and Goc populations were calculated, over the entire simulated time interval (usually of ≥10-s duration), so as to evaluate the contribution of Gocs to gain control. It readily became clear, however, that the feedback inhibition exerted by Gocs on grcs strongly influenced the degree of synchrony and rhythmicity in either neuron population. To explore this phenomenon, a synchronization index (SI) for cell populations was defined. All spikes from the neurons of a (grc or Goc) population (excluding neurons close to the network border) were compiled in 1-ms bins, producing a population spike time histogram (usually ≥10 s long; Fig. 3*B*). This histogram was autocorrelated, in 1-ms steps over a 0- to 1-s offset interval, generating a less noisy and zero-phased time series (Fig. 3*E*). The population SI is intended to express the modulation depth of this autocorrelogram (AC). To this end, a cosine's period T (accuracy 0.1 ms) was optimized to yield a maximal internal product with the AC. After normalization, the SI mapped onto the interval [0.0, 1.0]

$$\mathrm{SI} = \frac{\sum_{n=1}^{1,000} \cos\left(2\pi\frac{n\Delta t}{T}\right) AC(n\Delta t)}{\sum_{n=1}^{1,000} \mathrm{AC}(n\Delta t)}, \text{ with } \Delta t = 1\text{ms} \qquad (2)$$

A flat autocorrelogram yields a SI of 0.0 and expresses incoherent or irregular firing. The SI equals 1.0 when the neurons of a population fire exclusively at time intervals that are multiples of the period T, even when they do not fire in every cycle of the oscillation. Examples of autocorrelation histograms corresponding to different SI values can be found in Figs. 3*E*, 4, *C* and *D*, and 5*B*.

The SI is a combined metric of population synchrony and rhythmicity. We therefore also compiled population interspike-interval histograms (ISIs), which counted the occurrences of intervals between two consecutive spikes in every neuron of the population, as an independent measure of rhythmicity (Fig. 3*C*). As an independent measure of synchrony, spike time histograms of individual neurons were cross-correlated (Fig. 3*D*).

RESULTS

We demonstrate how the grc and Goc populations, connected in a feedback circuit, became entrained in a very regular, clock-like firing pattern as soon as the grcs received random MF input. Nonoscillatory behavior, on the other hand, could be observed when the average MF firing rate was very low, when monosynaptic MF input became the very dominant source of excitation of Gocs, and when the unitary inhibitory postsynaptic currents (IPSCs) of grcs became masked by a tonic activation of their $GABA_A$ channels. It further will be shown how the particular synaptic organization of the granular layer added to the accuracy of the model oscillations.

Dynamics of the granule cell ↔ Golgi cell feedback circuit

The grcs and Gocs started firing rhythmically and synchronized when the grcs received excitation from randomly spiking MFs and when the Gocs were predominantly excited through PF synapses. This behavior is demonstrated in the standard model in Fig. 3. The spontaneously firing Gocs synchronized their spikes within 20 ms after the start of MF activity (see rasterplot in Fig. 3*A*). Once synchronized, the Gocs fired almost every 46 ms, resulting in a very sharp peak in their population ISI histogram (Fig. 3*C*). At the same time, the grcs also synchronized but less prominently than the Gocs (compare their respective cross-correlograms in Fig. 3*D*). The weaker synchrony of grcs was reflected in a less sharp population spike time (Fig. 3*B*) and autocorrelation histogram (Fig. 3*E*). The synchronization of grcs was less pronounced because individual grcs fired less regularly than Gocs, as revealed by a broader ISI histogram (Fig. 3*C*). Grcs also did not fire every cycle, resulting in peaks in their ISI histogram at integer multiples of the 46-ms oscillation period.

The high stability of this oscillatory firing pattern was evident from the following control simulations. First, a spike train of the same frequency and duration, generated by an

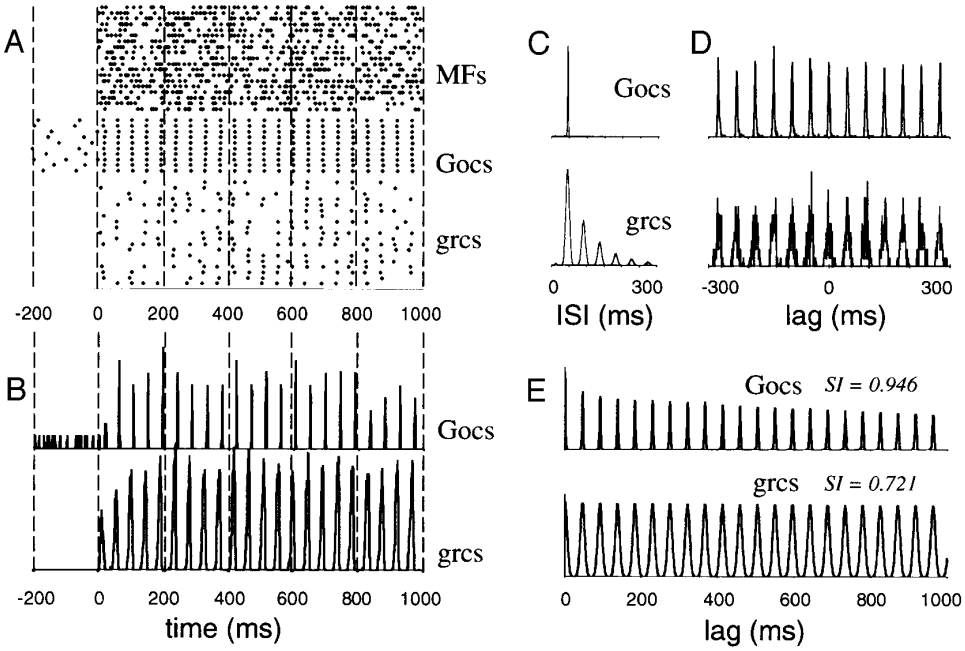

FIG. 3. Analysis of typical responses of the standard model. In the rasterogram (*A*), each dot indicates a spike occurrence. *Middle 10 rows* depict the central 10 Gocs. *Top* and *bottom rows* correspond to 19 MFs and grcs, respectively, lying at the same positions as the Gocs and at positions halfway in between them. Hence, this rasterogram spans 2.7 mm along the PF axis. To demonstrate the fast transition to synchronous firing, the network first is shown without MF input, with only the Gocs firing spontaneously. Population spike time histograms (*B*) and their autocorrelograms (*E*) for the Goc (*top rows*) and grc populations (*bottom rows*) were computed as explained in METHODS. Regularity of firing can be assessed from the population interspike interval (ISI) histograms (*C*). Synchronicity is demonstrated independently from the cross-correlograms between the spike trains of separate neurons, as shown in *D* for the couple of Gocs (*top*) and the couple of grcs (*bottom*) lying at the outermost positions of the rasterogram in *A*.

isolated model Goc injected with a constant 27.5-pA current, had a SI of 0.961 (compare with 0.946 in Fig. 3*E*). Second, when the entire grc population received exclusively inhibition from a single perfectly regularly firing interneuron, its SI measured 0.762 (0.721 in Fig. 3*E*).

Strength of synaptic coupling between Golgi and granule cells

The regular and synchronized firing pattern was produced by the feedback coupling between the grc and Goc populations. Figure 4, *C* and *D*, demonstrates how, as a consequence, the synchronization indices (SIs) rose when the synapses involved in the feedback coupling (the Goc inhibition of grcs and the PF excitation of Gocs) were increased in strength. The abrupt fall in SI at high strengths of PF excitation corresponded to the network operating in an unphysiological range of parameters (see legend of Fig. 4*D*).

The effects on the average population firing rates produced by altering the peak conductances of these synapses were more complex as Gocs and grcs reacted differently. These effects can be most easily understood by a linear systems analysis of the lumped circuit (Fig. 1*A*). If we let *mf*, *Go*,

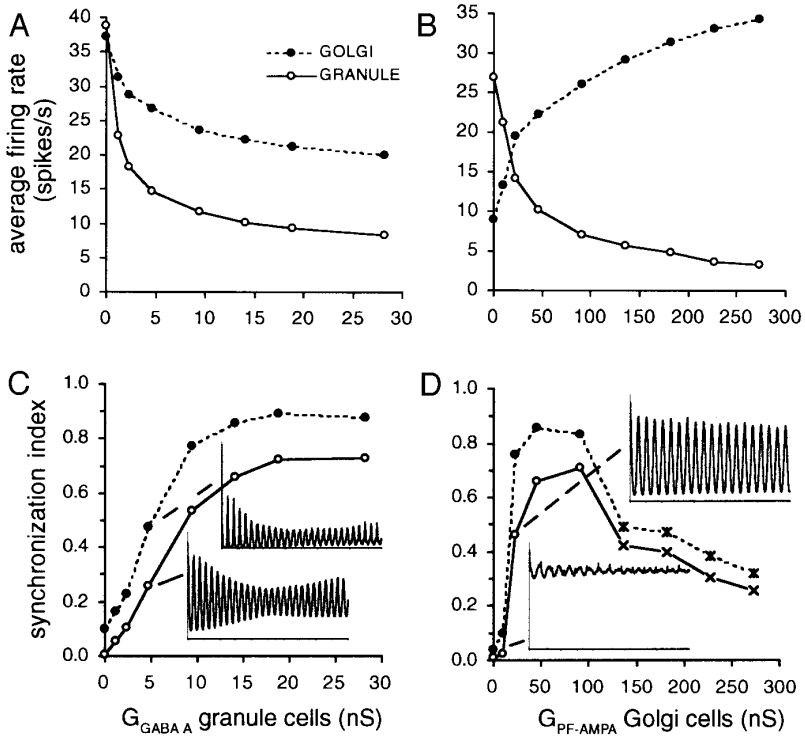

FIG. 4. Effects of the synaptic weights in the Goc-grc feedback circuit on network dynamics. Average firing rates (*A* and *B*) and SIs (*C* and *D*) of the Goc (– – –) and grc populations (——) are shown as functions of the synaptic strength of the Goc inhibition of grcs (*A* and *C*) and of the PF excitation of Gocs (*B* and *D*). Synaptic strengths are expressed as global peak conductances (see METHODS, *Synaptic weights*). Simulations of the standard model with 90 MFs, 4,662 grcs, and an average number of 560 PF synapses per Goc. In *A* and *C*, the PF-activated AMPA channel of Gocs had a global peak conductance of 45.5 nS, whereas the global peak conductance of the $GABA_A$ channel of grcs measured 14.1 nS in *B* and *D*. *Insets* in *C* and *D* show, for the indicated SI values, the corresponding autocorrelograms of the population spike time histograms (0- to 1-s time axis; compare with Fig. 3*E*). At global peak conductances of the PF to Goc synapses larger than 100 nS (crossed data points in *D*), Gocs fired doublets of spikes (with a 3 ms ISI). This type of firing which has never been observed during in vivo recordings of Goc activity (Atkins et al. 1997; Edgley and Lidierth 1987; Ito 1984; Van Kan et al. 1993; Vos et al. 1997) caused a decrease of the SI.

and *gr* be scalars denoting the average firing activity of the MF, Goc, and grc population respectively, and $K_{Go\rightarrow gr}$ and $K_{gr\rightarrow Go}$ be the average connection weights, then the following steady-state solution holds

$$gr = \frac{mf}{1 + K_{Go\rightarrow gr} \cdot K_{gr\rightarrow Go}} \quad (3)$$

$$Go = \frac{mf \cdot K_{gr\rightarrow Go}}{1 + K_{Go\rightarrow gr} \cdot K_{gr\rightarrow Go}} \quad (4)$$

The average steady-state firing rate of grcs decreased hyperbolically when the feedback inhibition grew stronger (*Eq. 3*), irrespective of whether a stronger feedback coupling was caused by a larger conductance of the $GABA_A$-mediated synapses that grcs received from Gocs ($K_{Go\rightarrow gr}$, Fig. 4*A*) or by a larger conductance of the AMPA-mediated synapses which PFs made on Gocs ($K_{gr\rightarrow Go}$, Fig. 4*B*). The average steady-state firing rate of Gocs similarly was a hyperbolically decreasing function (*Eq. 4*) of $K_{Go\rightarrow gr}$ (Fig. 4*A*), but it increased, as a Michaelis-Menten function (*Eq. 4*), when the PF synapses grew stronger ($K_{gr\rightarrow Go}$, Fig. 4*B*). In other words, while increasing $K_{Go\rightarrow gr}$ had similar effects on grc and Goc firing rates, increasing $K_{gr\rightarrow Go}$ had opposite effects.

Combining the information in all panels of Fig. 4, it is clear that the stronger grc firing was being suppressed, the more regular and synchronized became the grc (and Goc) firing pattern. Although the exact strengths of the synapses involved are not known experimentally, it must be concluded that if the feedback inhibition from Gocs to grcs really serves to restrict the number of active PFs, as suggested by standard theories of cerebellar function (Braitenberg et al. 1997; Marr 1969), then oscillations inevitably will be induced.

Mossy fiber excitation of Golgi cells

In the standard model presented so far, Gocs received excitation through PF input only. However, actual Gocs also receive monosynaptic excitation from MFs, which make synapses on their cell bodies and basal dendrites (Palay and Chan-Palay 1974). Although the PF synapses seem to outnumber the MF synapses (Pellionisz and Szentágothai (1973) used a ratio of 4,788 to 228), the EPSPs evoked by electrical stimulation of the white matter are, in vitro, larger than those evoked by stimulation of the molecular layer, probably due to the more central positioning of MF synapses on Gocs (Dieudonné and Kehoe 1996).

The effect of monosynaptic MF excitation of Gocs, and of the concomitant feedforward inhibition of grcs (Fig. 1*A*), was evaluated with the feedforward-inhibition model (see METHODS). The global peak conductance of the MF-activated AMPA channel of Gocs was varied from 0 to 200% relative to the PF-activated AMPA channel, the global peak conductance of which was kept constant at 45.5 nS. In addition, by using two different degrees of MF-to-Goc convergence, the global peak conductance of the MF-activated AMPA channel became distributed over 18 or 108 MF synapses onto each Goc. Together, these parameter combinations captured the above-mentioned differences between actual MFs and PFs in the numbers and strengths of their synapses.

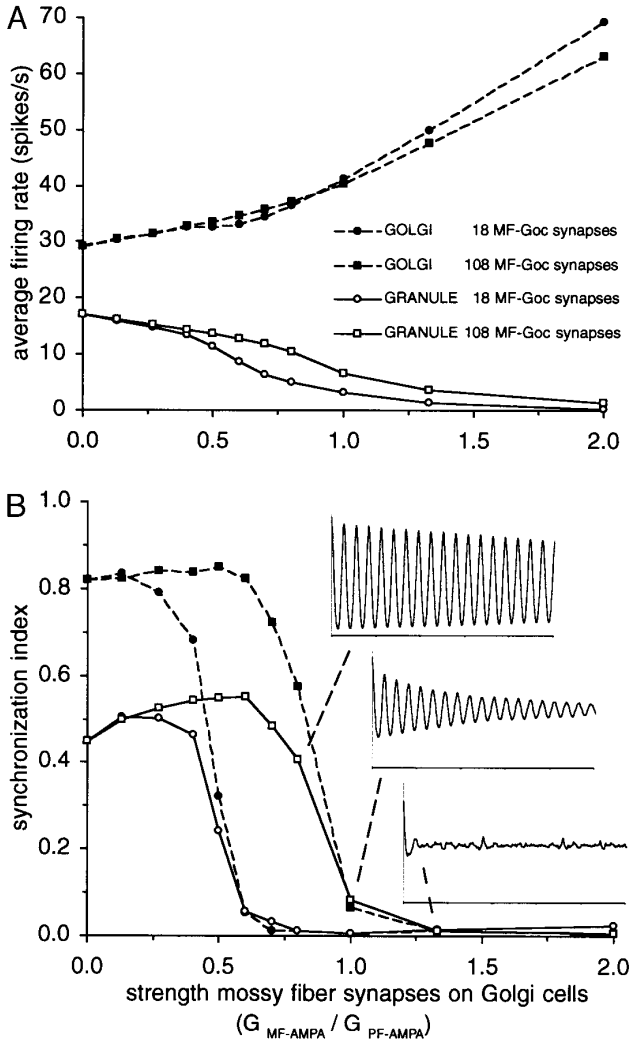

FIG. 5. Effects of feedforward inhibition of grcs on network dynamics. Firing rates (*A*) and SIs (*B*) of Gocs (– – –) and grcs (——) are plotted vs. the global peak conductance of the MF-activated AMPA receptor channel of Gocs, which is expressed relative to the global peak conductance of the PF-activated AMPA channel. There were 1 or 6 Gocs postsynaptic to every MF, corresponding to 18 or 108 MF synapses on every Goc, respectively. *Insets*: autocorrelation histograms (0- to 500-ms time axis) of the grc population (curve □) at values of 0.8, 1.0, and 1.3 on the abcissa (compare with Fig. 3*E*).

Figure 5*B* shows that the SIs remained unaffected or even slightly rose by increasing the level of MF-to-Goc excitation, until a clear threshold was reached above which the randomly spiking MFs tended to increasingly desynchronize the Gocs and hence the whole network. It is straightforward that the coherence built up through correlated PF inputs became disrupted by the random firing of the MF inputs. However, when the number of MF synapses was increased and each individual synapse had, due to the normalization procedure (see METHODS), a proportionately smaller weight, the oscillations persisted at much stronger levels of MF-to-Goc excitation (compare the curves for 18 and 108 MF synapses).

The autocorrelation histograms in Fig. 5*B* illustrate these findings: the oscillations became less accurate and more transient when the relative strength of the MF-activated AMPA

channel was increased from 0.8 to 1.0. At a relative strength of 1.3, the oscillations disappeared completely. Note, however, that when the relative firing rates of MFs (40 spikes/s) and PFs (see Fig. 5*A*) were taken into account at these different synaptic strengths, the latter two autocorrelograms corresponded to an overall MF excitatory input that was 6 and 15 times stronger than the input through PFs. Hence, the oscillations in the model granular layer persisted even when >85% of the excitatory input to Gocs was provided by way of MFs (relative synaptic strength of 1.0).

Finally, Fig. 5*A* shows that the average firing rate of grcs decreased almost linearly with the strength of MF excitation of Gocs and did not stabilize toward a lower limit. In this aspect feedforward inhibition was more efficient than feedback inhibition at restricting the number of active PFs.

Mossy fiber excitation of granule cells

The average MF firing rate was an important controlling parameter for the network oscillations. First, an increased MF firing rate enhanced the firing rate of both grcs and Gocs (Fig. 6*A*). This always occurred by a shortening of their oscillation periods, never by a transition to doublet or burst firing. Hence the frequency of the oscillations varied in the standard model between 12 Hz for an average MF firing rate of 10 spikes/s and 44 Hz for 260 spikes/s. The corresponding oscillation periods ranged from 23 to 82 ms (Fig. 6*A*), which is in agreement with the 20- to 80-ms range of modal interspike intervals measured for different Gocs in behaving cats (Edgley and Lidierth 1987).

Second, synchrony required a minimum average firing rate of MFs: the oscillations almost completely disappeared at <10–15 spikes/s (standard model, Fig. 6*B*). This loss of rhythmogenesis can be explained by the progressive increase in oscillation period (Fig. 6*A*), which eventually would last longer than the IPSP evoked in grcs by a single Goc spike. As a consequence, MF-triggered grc spikes and spontaneous Goc spikes escaped from the rhythm. The network still oscillated at lower frequencies when a slower kinetics for the $GABA_A$ channel of grcs was used.

Similar results were observed in the feedforward-inhibition model for MF firing rates of 20–40 spikes/s (Fig. 6*C*). At higher MF firing rates, the curves of Fig. 6*C* became more complex because Gocs received monosynaptic MF excitation at increased rates as well. It is important to note that in Fig. 6*C*, the peak conductances of both the MF- and PF-activated AMPA channels of Gocs were reduced in strength by 50% to diminish the firing of doublets by the Gocs (see Fig. 4*D*, legend). This simple reduction in total excitatory input sufficed to raise the SI from 0.013 in Fig. 5*B* to >0.5 in Fig. 6*C* for a relative MF synaptic strength of 1.3 (40 spikes/s). Hence the decline in SI in Fig. 5*B* was caused partly by an overexcitation of the model Gocs, probably beyond physiological levels.

Finally, we also compared the contributions of the AMPA- and NMDA-receptor channels at the MF-to-grc synapses (D'Angelo et al. 1995). It appeared that NMDA channels, although not essential for the generation of network oscillations, had a strongly stabilizing effect. They contributed more than AMPA channels to grc excitation (Fig. 2*C*), but because of their slow time course and low peak amplitude, they damped the jitter in the input caused by the randomly activated MFs.

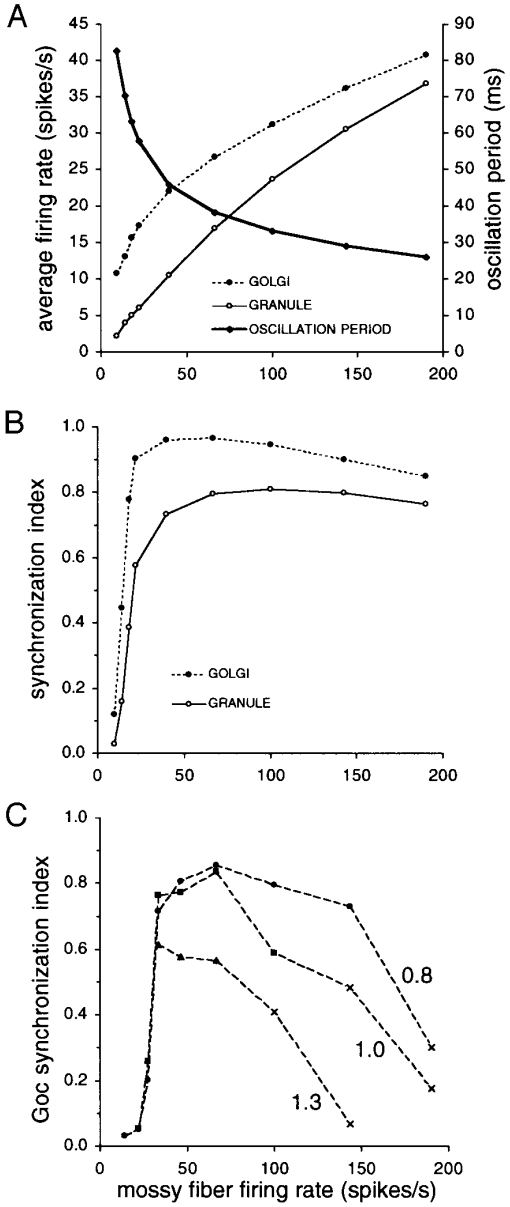

FIG. 6. Effects of MF firing rate on network dynamics in the standard model (*A* and *B*) and in the feedforward-inhibition model (*C*). Average firing rates (*A*) and SIs (*B*) of Gocs (– – –) and grcs (——) in the standard model are plotted as functions of the average firing rate of MFs. All MFs in the network fired at the same average rate. The diamonds in *A* indicate the oscillation period (right vertical axis). In *C*, the feedforward-inhibition model was simulated at 3 relative strengths of MF excitation of Gocs (0.8, 1.0, and 1.3, i.e., the same strengths for which autocorrelograms are shown in Fig. 5*B*). Global peak conductances of both AMPA channels of Gocs were reduced by 50% to prevent that Gocs would fire doublets. Nevertheless, at high MF firing rates, the Gocs still fired >10% of their spikes <10 ms after a previous spike (crossed data points).

Numbers of mossy fibers, granule cells, and parallel fiber synapses

We demonstrate now, by means of the standard model, that the numbers of MFs and grcs, as well as the average

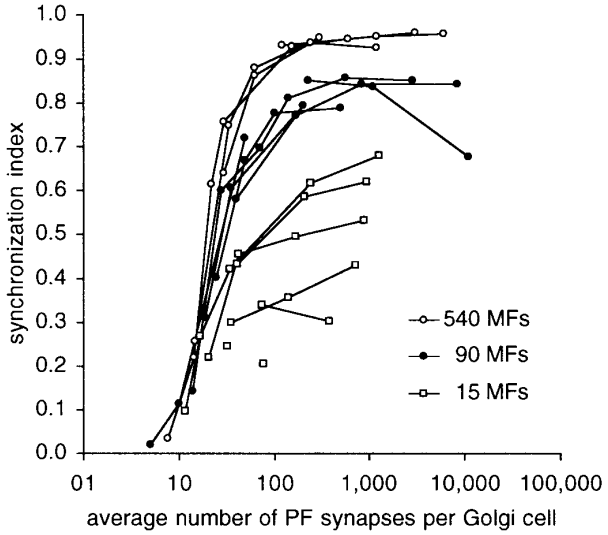

FIG. 7. Effect of the average number of PF synapses on Gocs on the SI of the Goc population. Data were computed for the standard model but using varying numbers of MFs, varying numbers of grcs, and varying connection probabilities *P* from grcs to Gocs. Because Gocs at the edges of the circuit have less PFs to be connected by, the number of PF synapses was averaged over the central 10 Gocs only. As explained in METHODS, this number of PF synapses was defined by 2 network parameters: the number of grcs and the PF-to-Goc connection probability *P*. The number of grcs in turn was varied over several orders of magnitude by altering either the span value *S* for MF ramification or the number of MFs itself (see *Eq. 1* and Fig. 1*B*). Each curve connects data points obtained from networks with the same numbers of grcs and MFs but varying values of *P*. They represent networks with 45, 105, 462, 810, 990, 1,155, or 1,365 grcs and 15 MFs (□), networks with 87, 345, 855, 4,662, 13,365, or 17,655 grcs and 90 MFs (●), and networks with 537, 2,145, 5,355, or 10,695 grcs and 540 MFs (○). Isolated points and the rightmost point on each curve are from maximally connected networks ($P = 1.0$). Because the number of PF synapses in a maximally connected network is proportional to the number of grcs, these points can be used to rank the curves by increasing numbers of grcs.

number of PF synapses per Goc, were critical factors in the synchronization process and that the granular layer of the cerebellum satisfies these constraints. The average firing rates of grcs and Gocs, on the other hand, hardly were affected by changing these numbers because the global peak conductance of the PF-activated AMPA channel of Gocs was kept constant at 45.5 nS to dissociate the effect of the synaptic number from the above-described effect of the global peak conductance (Fig. 4*D*).

Figure 7 plots how the SI of the Goc population depended on the average number of PF synapses per Goc and on the numbers of MFs and grcs. Each curve connects the SIs obtained from networks with fixed numbers of MFs and grcs but different connection probabilities *P* from grcs to Gocs. Different curves are from networks with different numbers of MFs and/or grcs (see legend). It can be seen that all SI curves were quite similar Michaelis-Menten-like functions of the number of PF synapses. The curves differed only in the asymptotic values reached, which depended more on the number of MFs than on the number of grcs. Indeed, curves from networks with different numbers of MFs were largely nonoverlapping, while within a set of networks with the same number of MFs, curves were much less separated (except in the 15 MF networks).

As an illustration of these principles, a model with 540 MFs and an average number of 62 PF synapses on every Goc produced a Goc SI of 0.881 when there were 537 grcs ($P = 0.2$) and of 0.864 in a model with 2,145 grcs ($P = 0.05$). But the highest value of the SI obtained for a similar number of PF synapses was only 0.457 in models with 15 MFs (42 PF synapses, 995 grcs, $P = 0.05$) and 0.699 in models with 90 MFs (70 PF synapses, 4,662 grcs, $P = 0.025$). In the 15-MFs network set, the asymptotic value of the SI increased with the number of grcs from 0.431 (810 grcs, $P = 1.0$, 704 PF synapses) to 0.68 (1,365 grcs, $P = 1.0$, 1,239 PF synapses).

At densities of ~20 PF synapses onto each Goc, all curves reached SI levels of approximately half their asymptotic values (Fig. 7). Hence, a small number of PF synapses sufficed for achieving remarkably high SIs, even in networks with thousands of grcs of which only a fraction made PF synapses on the 30 available Gocs. It follows that if grcs were densely connected to Gocs (large numbers of PF synapses), then only a fraction of them would need to be activated by MF input to synchronize the network. We conclude that large numbers of MFs and grcs added to the accuracy of the oscillations (Fig. 7) but that synchronization could be sustained in networks with a sparse grc activity.

The actual values of the parameters varied in this section are not accurately known. Nevertheless, Ito (1984) estimated a ratio of four MFs per Purkinje cell in the white matter of cat cerebellum, and in the same animal, the Purkinje/Goc ratio measures 3.2 (Palkovitz et al. 1972), making 540 MFs in a circuit of 30 Gocs a realistic figure. In addition, given that the excitatory postsynaptic currents evoked by spontaneous PF activation measure 38 pA at the soma of rat Gocs clamped at −70 mV (Dieudonné 1998), our global peak conductance of 45.5 nS for the PF-activated AMPA channel corresponded, in retrospect, to the cumulative activation of 84 PFs, which is, from the analysis of Fig. 7, quite sufficient to generate robust oscillations.

Parallel fiber conduction speed

The synchronization of Gocs over a distance of several millimeters (Fig. 3*A*) was remarkable given the low PF conduction speed. While it appears from Fig. 8 that our standard value of 0.5 m/s was almost optimal in this respect, synchronization remained prominent for speeds as low as 0.1 m/s (speed^{-1} 10 s/m). Note that at this speed the delay between activation of the most proximal and distal PF synapse comprised 25 ms or as long as 44% of the oscillation period. Moreover, randomizing the timing of PF excitation of Gocs by distributing the delays of the PF synapses uniformly in ±100% intervals around their standard values did not have any deteriorating effect on synchronization.

Although varying the PF conduction speed within physiological ranges (Bernard and Axelrad 1991; Eccles et al. 1966; Vranesic et al. 1994) did not affect the SI much, it did have an effect on the oscillation period by changing the delay of the feedback loop. As shown in Fig. 8, the oscillation period increased in reverse proportion to the PF conduction speed and hence proportional to the conduction delays from grcs to Gocs.

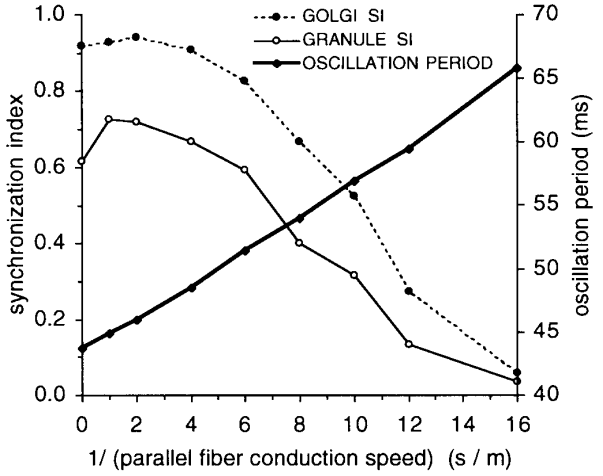

FIG. 8. Effects of PF conduction speed on the SIs of Gocs (– – –) and grcs (——), and on the network oscillation period (♦, right vertical axis). Simulations of the standard model. Data are plotted vs. the inverse of PF conduction speed, which is proportional to the ensuing grc to Goc conduction delays. Oscillation period was defined as the value of T in *Eq. 2* (see METHODS) and corresponded also to the peak ISI of either neuron population. All other results in the present study have been obtained from networks with a conduction speed of 0.5 m/s (speed^{-1} 2 s/m).

Golgi cell inhibition of granule cells

In Fig. 4, *A* and *C*, we have demonstrated that the global peak conductance of the $GABA_A$ channel of grcs is a critical parameter, for network synchronization as well as for gain control. Unfortunately, a reliable in vivo estimate of this parameter is not on hand. In adult rats in vitro, grcs display spontaneous, bicuculline-sensitive, unitary currents of 600 pA (Brickley et al. 1996), but it is unclear how many of the ~10 inhibitory synaptic contacts on grcs (Jakab and Hámori 1988) actually are activated during a unitary IPSC. Indeed, a major problem in interpreting these IPSC amplitudes is that the inhibitory synapses on grcs originate from an unknown number of Gocs because the axonal plexuses of Gocs overlap to some extent (De Zeeuw et al. 1995; Palay and Chan-Palay 1974). In this respect, the model predicts that if the inhibitory synapses on a grc originate from more than one Goc, then the relative timing of their activation determines the degree of grc suppression and this suppression will be much more profound the more asynchronously the afferent Gocs fire (data not shown). This is another instance of the association between desynchronization and low PF (grc) firing rate (see also Figs. 5, 6, and 9).

Recently, a tonic Cl^- current has been recorded in grcs of adult rats in vitro (Brickley et al. 1996; Kaneda et al. 1995; Wall and Usowicz 1997). This inhibitory current passes through a bicuculline-sensitive channel with a conductance of a few hundred pS and carries a charge much larger than the total charge transferred by spontaneous, unitary IPSCs. We incorporated this in vitro finding in the model by providing all grcs with an additional, tonic GABA receptor channel (see *Tonic-inhibition model* in METHODS). Through temporal summation, these tonic channels reached steady-state conductances of ≤1,400 pS.

Figure 9*A* shows that the average firing rates of grcs and Gocs decreased almost linearly with the steady-state conductance of the tonic GABA channels until levels of spontaneous activity were reached (0 for grcs and 8.8 spikes/s for Gocs). Nevertheless, the synchronous oscillations persisted provided the MF input was sufficiently strong (Fig. 9*B*). For example, when the MFs fired at rates of 100 spikes/s, the SIs remained unaffected by a tonic Cl^- conductance as high as 950 pS (Fig. 9*B*), which is much higher than the 150–300 pS actually measured in vitro. Interestingly, when the data from *A* and *B* were combined, the fall in SI was related to a reduction in PF firing rate, independent of the strength of tonic inhibition itself.

It must be noted, however, that Gocs, which are the sole possible source of synchronizing and rhythmic input to grcs, still needed to activate the ''transient'' $GABA_A$ channels of grcs with an appreciable frequency for synchronization to ensue. For example, in the network producing a Goc SI of 0.853 at a tonic inhibition of 951 pS (Fig. 9*B*, curve for 100 spikes/s MF firing rate), unitary $GABA_A$-channel-mediated IPSCs still accounted for 39% of the inhibitory current in grcs. An almost complete absence of unitary IPSCs, as has been reported in adult rats in vitro (Wall and Usowicz 1997), precludes the emergence of synchronized and rhythmic firing in grcs and hence in the entire network.

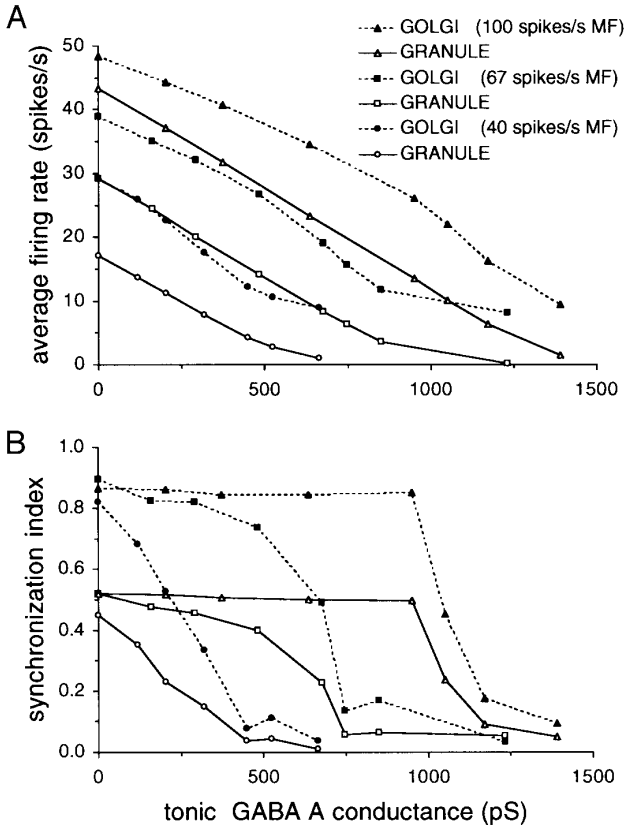

FIG. 9. Effects produced by a tonic inhibition of grcs. Average firing rates (*A*) and SIs (*B*) of Gocs (– – –) and grcs (——) in the tonic inhibition model. Networks with 40 Hz (○), 67 Hz (□), and 100 Hz (△) MF input are compared. Data are plotted vs. the average conductance of the tonic GABA channel of grcs, which depended on its global peak conductance (which was varied from 0 to 533 pS) and on the Goc firing rate (which depended primarily on the MF firing rate).

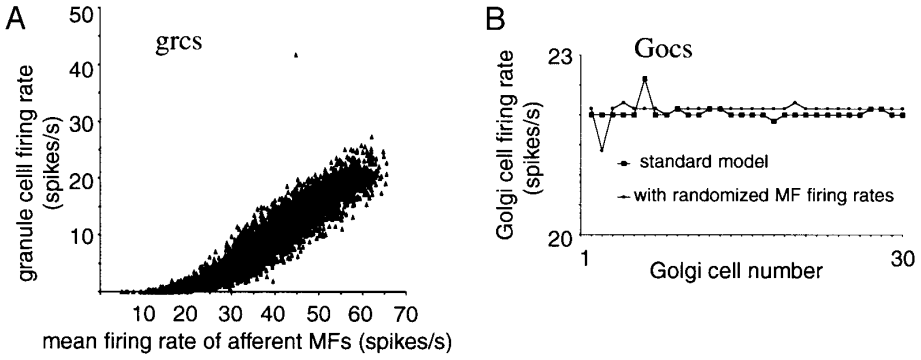

FIG. 10. Effects produced by increasing the variability of the rate of MF input to grcs in the standard model. In the scatter plot of *A*, the average firing rate of each grc is plotted against the mean firing rate of its individual set of four afferent MFs. Note that the isolated point corresponds to a grc that inadvertantly did not have a Goc afferent, and hence it can be used to assess the effect of inhibition. In *B*, it is demonstrated that the variability in average firing rate among Gocs did not increase with the extra randomization of the MF input. Increased variability of the MF input was realized by distributing the average firing rate of individual MFs uniformly between 5 and 75 Hz.

Robustness of the model oscillations to additional parameter randomization

Although the isolated model Gocs and grcs, owing to their large sets of voltage-gated channels, reliably reproduced the dynamics of actual slice Gocs and grcs (Fig. 2), predicting network interactions could be argued to require a detailed representation of the dendrites. We tried to capture the effects of putting synapses at different positions on a passive dendritic tree by extending the randomization intervals of the synaptic time courses, delays, and weights. The following results demonstrate the extreme robustness of the synchronous, rhythmic firing pattern.

To test the effect of variability in the time course of individual synapses, the decay time constant (τ_2) of each synaptic channel as well as the synaptic delay of each afferent was substituted with random values between 50 and 150% of their standard values. As we did not use a delay for the Goc-to-grc synapses, a 2-ms delay was added here. Furthermore, to test the effect of unequal strengths of synaptic activation, the distribution intervals of the synaptic weight factors and of the global peak conductances of the postsynaptic channels were extended to $\pm 50\%$ (compared with $\pm 15\%$ in the standard models), either for all types of channels simultaneously or for each channel type in isolation. Surprisingly, with only a single exception, these randomizations hardly affected network synchrony and rhythmicity at all, i.e., the SIs remained >0.9 for Gocs and >0.6 for grcs (compare to Fig. 3*E*). The one exception was the global peak conductance of the PF-activated AMPA channel of Gocs. If this conductance was randomized to a level where the differences in excitation between individual Gocs became very large (more than threefold), the entire network desynchronized and each Goc started firing at its own rate.

Finally, we also tested the sensitivity of the model to a larger variability in the MF input to individual grcs by assigning each MF a separate average firing rate, chosen randomly between 5 and 75 spikes/s. The mean firing rate of the MF population remained at 40 spikes/s, but its variability was probably closer to the situation in vivo and caused a broad distribution of grc average firing rates (Fig. 10*A*). Nevertheless, synchrony and rhythmicity were hardly affected (Goc SI = 0.926, grc SI = 0.654, compare to Fig. 3*E*). This can be explained by the massive convergence of grc inputs onto Gocs. Because Gocs sampled through PF synapses the activity of hundreds of grcs, the variability in firing rate among Gocs did *not* increase concomitantly with the variability of the grc firing rate (compare the firing rate distributions in Fig. 10, *A* and *B*), and a single rhythm was imposed on the entire network (Maex and De Schutter 1998).

DISCUSSION

Rather than trying to reproduce experimental data, which unfortunately are hardly available, this modeling study was explorative in nature. Nevertheless, the observation that the Golgi cell-granule cell feedback loop can act as an oscillator under conditions of random MF input deserves the attention of both experimentalists and theoreticians. A clocklike, synchronous firing pattern emerged when the Gocs received excitation predominantly through PFs but could proceed to an asynchronous firing pattern when the MF input to Gocs was increased in strength. These opposing effects of PF versus MF input to Gocs are discussed first, as the relevance of our model oscillations for cerebellar functioning depends on the existence of a circuit providing Gocs with a sufficiently strong PF excitation. We next underscore the reliability of our observations by showing that the architecture of the granular layer resembles, in many respects, that of neuronal network models of oscillatory behavior. It also is argued that this behavior is not an artificial dynamic phenomenon due to limitations of the model or the use of unrealistic parameters. Finally, we discuss the model predictions and its implications for the function of Gocs and of the cerebellum (De Schutter and Maex 1996).

Parallel fiber versus mossy fiber excitation of Golgi cells

Three principles adequately describe the effect of Goc excitation on network synchrony. First, whenever Gocs are very strongly excited, synchrony deteriorates either because Gocs fire doublets (an unphysiological condition, see Figs. 4*D* and 6*C*) or because they suppress PF firing almost completely (Fig. 5*B*). Second, for a given level of Goc excitation, the SI sharply declines when the contribution of MFs to excitation grows above a threshold fraction (Fig. 5*B*). However, a 10 times stronger MF than PF input may be needed to desynchronize the entire network. Third, this threshold fraction increases with the number of MF afferents to Gocs. A similar threshold effect holds for the number of PF synapses on Gocs (Fig. 7).

Because not only the relative numbers of MF and PF synapses but also their absolute numbers are important according to these principles, there is a need for quantitative anatomic data on the innervation of Gocs. An additional

problem in predicting the stability of oscillations in vivo is that only a fraction of the synapses might be activated depending on the MF activity pattern.

Physiological data, however, indicate that the requirements for synchronization may be fulfilled in vivo. First, in vivo recorded Gocs typically do not fire with intervals <10 ms, and their slow firing rates are only modestly modulated in response to motor activity (Edgley and Lidierth 1987; Miles et al. 1980; but see Van Kan et al. 1993). Second, although PF synapses have a lower efficacy than MF synapses, Dieudonné (1998) estimated that activation of as few as 40 PF synapses would suffice to evoke a Goc spike, which is similar to the putative number of 50 PFs for Purkinje cell excitation (Barbour 1993). Finally, Vos et al. (1997) found in anesthetized rats strongly correlated firing between Gocs aligned along the PF axis but not along the sagittal axis.

Together, these data suggest that Gocs are indeed excitable through PF input and that this input evokes a considerable number of Goc spikes. Hence, the PF pathway of Goc excitation might be strong enough to support synchronization and rhythmogenesis.

Unique structure of the cerebellar granule cell layer

The critical components that support oscillations in the present model are the PF excitation of Gocs, which coupled the Gocs in a synchronous rhythm, and the feedback inhibition to grcs, which coupled the grc rhythm to that of Gocs. Although this mechanism is not fundamentally different from the oscillatory mechanism in models of other brain areas, several features of its anatomy make the granular layer more liable to oscillations than other structures like hippocampus and cerebral cortex.

ABSENCE OF GRC-GRC AND GOC-GOC SYNAPSES. The populations of excitatory (grcs) and inhibitory neurons (Gocs) are reciprocally connected, but the absence of synapses among grcs and among Gocs is unique. Indeed, Freeman (1972) already recognized the oscillatory capability of circuits with this architecture, but he did not consider their existence in the vertebrate brain.

In general, synapses between the excitatory neurons of a population have a destabilizing effect on synchronization (Bush and Sejnowski 1996; Hansel et al. 1995; Traub et al. 1997). It is significant in this respect that König and Schillen needed to introduce lateral connections between the excitatory neurons of their cerebral cortex model to allow for a stimulus-specific *desynchronization* (Schillen and König 1991). On the other hand, excitatory synapses can be strongly synchronizing when the targets are inhibitory neurons (Bush and Sejnowski 1996) as in the present model.

In a recent hippocampal model, it was found that lateral inhibition alone can accomplish synchronization provided its time course is slow (Whittington et al. 1995). It can be argued that this latter mechanism of lateral, monosynaptic inhibition is not completely different from the one presented here. Indeed, the Gocs also inhibit one another slowly by indirect or polysynaptic coupling, i.e., by suppressing their mutual sources of excitation (the grcs). It is not surprising then that the oscillations in the present model were slower than in the hippocampus model (10–40 vs. 30–80 Hz). There are, however, some prominent differences between the two models. First, in the hippocampal model, synchronization of excitatory as well as inhibitory neurons is achieved almost completely through the common inhibitory input they receive. The spikes themselves are evoked through slow excitation, either through steady current injection or through synaptic activation of NMDA-receptor channels. In contrast, both common excitation (of Gocs) and common inhibition (of grcs) contributed to synchronization and rhythmogenesis in the present model. Second, when the excitatory neurons in the hippocampal model additionally are coupled to the inhibitory neurons through fast AMPA-mediated excitation, they evoke EPSPs that *lag* the inhibitory neurons' spikes (evoked through slow excitation) and trigger a secondary, doublet spike (Traub et al. 1997). Because only the secondary spikes of inhibitory neurons directly couple the rhythm of inhibitory neurons to that of excitatory neurons, it is not surprising that the occurrence of spike doublets considerably improves synchronization (Ermentrout and Kopell 1998; Traub et al. 1996). In contrast, the inhibitory Gocs in the present model fired, once the network was synchronized, through the pulsatile input they received from the excitatory grcs whose spikes *led* the Goc spikes by a few milliseconds. Doublet spikes in Gocs, arising either by a dominant MF excitation or by very strong PF synapses, consequently tended to perturb the rhythmic firing pattern (Figs. 4*D* and 6*C*).

NUMBERS OF MOSSY FIBERS, GRANULE CELLS, AND GOLGI CELLS. Synchronization scaled with the density of MFs (Fig. 7), and it is interesting to note that the cerebellum is characterized by an exceptionally high ratio of input fibers over output fibers (Brodal and Bjaalie 1992). Similarly, a large number of grcs, the most numerous neurons in the entire brain, supported the synchronization process. In particular, if only a small number of sparsely distributed MFs fires, then the fraction of activated grcs will be small and a large population of grcs will be needed to produce a set of active PFs large enough to entrain the oscillations (Fig. 7). Finally, because of the relative sparseness of the Gocs, the granular layer of the cerebellum almost perfectly matches the ''comparator circuit'' of Kammen et al. (1989). These authors demonstrate that a circuit with feedback coupling between a single inhibitory neuron and an array of excitatory oscillators is the network of choice for synchronizing these oscillators, performing much better than a network with lateral coupling. As such, the PFs in our model can be thought of as connecting and synchronizing an array of individual comparator circuits.

SLOW PARALLEL FIBER CONDUCTION SPEED. The finding that a 0.1- to 0.5-m/s PF conduction speed was fast enough to generate coherent firing (Fig. 8) implies a mechanism to circumvent axonal conduction delays as high as 5–25 ms. Two architectural features of the model granular layer prevent the occurrence of phase breaks in the chain of synchronously firing neurons. First, the numerous and long PFs ensure a massive convergence from grcs to Gocs and hence a large degree of overlap in excitation between Gocs. Second, the very densely packed grcs and the regularly spaced synapses on their PFs (Harvey and Napper 1991; Pichitpornchai et al. 1994) generate an almost uniform distribution of con-

duction delays to Gocs. This contrasts with models of columnar structures like the cerebral cortex, where intercolumnar delays are much larger than intracolumnar delays (Bush and Sejnowski 1996; see also Crook et al. 1997; Traub et al. 1996). In agreement with our findings, synchronization of a cerebral cortex model was very robust to variation and randomization of the synaptic delays *within* a column (Bush and Sejnowski 1996).

Limitations of the model and missing experimental data

NEURON MODELS. A simplification in the present work was the use of single-compartmental neurons. Given the robustness of the model oscillations to randomization of the weights, delays, and time courses of the individual synapses, however, it becomes improbable that passive filtering of synaptic inputs along multicompartmental dendrites will alter the dynamics of the network. Moreover, this approach has been applied successfully to models of many other brain regions (Destexhe et al. 1996; Golomb and Rinzel 1993; Jefferys et al. 1996; Manor et al. 1997; Wang and Buzsáki 1996) even when such models are not as robust to parameter randomization as the present model (e.g., Traub et al. 1997; Wang and Buzsáki 1996). Similarly, despite the absence of complete kinetic data on the different voltage-gated channels in rat grcs and Gocs, we believe that our model neurons captured the cellular properties of rat grcs (Brickley et al. 1996; D'Angelo et al. 1995; Puia et al. 1994; Silver et al. 1996) and Gocs (Dieudonné 1998) quite well. The importance of a faithful reproduction of the individual neurons' dynamics becomes clear when the clocklike spike trains emerging in the model Gocs and grcs are compared with the burst-like discharges of pyramidal and basket cells in a recent neocortex model (Bush and Sejnowski 1996).

SYNAPTIC ORGANIZATION. Besides using simplified model neurons, the network also did not include all known synaptic inputs to the granular layer. In particular, Gocs also receive input from climbing fibers, recurrent Purkinje axons (Palay and Chan-Palay 1974), and Lugaro cells (Dieudonné 1995), but only the slow inhibitory currents induced by stellate cells (stcs) have been described in some detail (Dieudonné and Kehoe 1996). Preliminary simulations demonstrate that input from stcs, activated by PFs, does not disrupt synchrony because the stc population becomes entrained in the rhythm. Even more, based on voltage-clamp recordings, stcs have been proposed recently to enhance rhythmic firing of Gocs (and consequently of grcs) by activating their H currents and eliciting postinhibitory rebound spikes (Dieudonné 1998). Finally, the robustness of the regular firing pattern to large variations in PF conduction speed (Fig. 8) and to randomization of the grc-to-Goc synaptic delays suggests that it will not be disrupted by the slight PF speed gradient that exists along the vertical axis of the molecular layer (Bernard and Axelrad 1991; Vranesic et al. 1994) but that was not included in the model.

MOSSY FIBER FIRING PATTERN. Our major concern in choosing the MF firing rates was to achieve in vivo levels of activity in the model granular layer, in which we apparently succeeded given the realistic firing rates of the model Gocs (Fig. 6*A*) (Edgley and Lidierth 1987; Miles et al. 1980; Van Kan et al. 1993). Actually, the pattern of MF activity in behaving animals is largely unknown, but Eccles et al. (1971) mention a ''resting'' impulse discharge of 20–100 spikes/s in lightly anesthetized cats, and Van Kan et al. (1993) measured tonic levels as high as 200 spikes/s during active arm movements in monkeys. Within this experimentally measured interval of average MF firing rates, stable oscillations almost invariably were observed in the model granular layer (Fig. 6, *B* and *C*), even when the individual MFs fired at different rates (Fig. 10). Although the average firing rates of the model MFs were realistic from the above, we do not intend to portray a stationary MF input as being true to nature. As argued in the INTRODUCTION, a stationary MF input was most appropriate to analyze how the model oscillations depended on network parameters.

TONIC INHIBITION OF GRANULE CELLS. Finally, a tonic inhibition of grcs desynchronized the network, but this effect could be neutralized completely by increasing the MF firing rate. It also remains to be proven that the spill-over of GABA in the MF glomerulus, which is the putative cause of tonic inhibition in grcs (Brickley et al. 1996; Wall and Usowicz 1997), is not an artifact of the in vitro preparation. Because $GABA_A$ receptors cluster at Goc-grc synapses (Nusser et al. 1995), the absence of unitary IPSCs and of any effect of tetrodotoxin application (Wall and Usowicz 1997) questions the normal functioning of Gocs in slices from adult rats (see also Dieudonné 1998).

Predictions of the model

The main prediction of the model is that the granular layer of the cerebellum can generate rhythmic and synchronized firing patterns in PFs. Because a sufficiently strong MF input is required for this purpose, the extent in space and time over which a single synchronous rhythm is measurable will be determined by the (largely unknown) natural pattern of MF input. Two groups recently have reported the presence of oscillations in the granular layer of awake monkeys (Pellerin and Lamarre 1997) and rats (Hartmann and Bower 1998). According to the present model, these oscillations may be generated in situ. The pauses in between oscillatory activity could be caused by a drop in MF activity or, alternatively, by a selective increase in activity, through an unknown mechanism, of the MFs providing monosynaptic excitation to Gocs.

In addition, the model makes four predictions about the dynamics of the granular layer, which should be verifiable through multiunit recordings from MFs, Gocs, and grcs. First, the more regular the rhythm produced by single Gocs (as assessed from their ISI histograms), the more synchronized pairs of Gocs should fire (as assessed from their cross-correlograms). This follows from the fact that rhythmicity arises at the network and not at the neuronal level. Actually, single putative Gocs have been reported to fire regularly (Armstrong and Rawson 1979; Edgley and Lidierth 1987; Van Kan et al. 1993), and this characteristic even has been used as a criterion for their identification (Miles et al. 1980). That Goc ISI histograms are broader in experimental studies than in our present modeling study seems inevitable given the sensitivity of both the oscillation period (Fig. 6*A*) and the SI itself (Fig. 6, *B* and *C*) on the strength of MF activity,

which can be expected to fluctuate during the recording period in behaving animals and to be tonically depressed in anesthetized animals. Our paired recordings of Goc activity, which we started subsequent to the results of the present study, confirm that most Goc pairs along the PF axis show significant synchronicity of firing in vivo, which is modulated by stimulation (Vos et al. 1997).

Second, if Gocs fire rhythmically and synchronized, then grcs should do the same. It is exciting in this respect that Eccles et al. (1971) were surprised to find, in the granular layer of lightly anesthetized or decerebrate cats, ''a considerable number of regularly rhythmic spike potentials,'' mostly of ~20 Hz, the source of which they could not identify. On the basis of the results from our study, we would attribute this activity to grcs.

Third, because synchronous and rhythmic firing becomes more prominent when the MF input grows stronger (Fig. 6, *B* and *C*), these properties should be more easily detectable in the awake, behaving animal. The oscillation frequency as well as the power of the frequency spectrum should thereby increase (Fig. 6*A*).

The final prediction stems from simulations of 2D versions of the network model. The 2D network extension did not affect the synchronicity established between neurons along the PF axis (data not shown). Along the sagittal axis, however, shared PF input between neighboring Gocs was restricted by the limited overlap of their dendritic trees, and consequently synchronization became less accurate with increasing distance. Hence a pair of Gocs lying along a PF axis should fire more synchronized than a pair lying along a sagittal axis, although the Gocs of both pairs could fire rhythmically. This latter prediction has been confirmed by Vos et al. (1997).

Functional implications

The general conclusion of this modeling study is that the granular layer of the cerebellum might be designed as a rhythm generator. Because MFs are the terminal axons of pathways originating from large parts of the nervous system (Brodal and Bjaalie 1997; Ito 1984), the average state of neural excitation could set the pace of the rhythm. More probably, fractured MF receptive fields (Bower and Kassel 1990; Shambes et al. 1978) could cause local territories of synchronization to wax and wane in the granular layer, transforming transiently enhanced activity at remote sites of the nervous system into pulsatile, rhythmic firing patterns.

The Gocs are, unlike inhibitory neurons in other systems like visual cortex (Maex and Orban 1996), too scarce and lack interconnections needed to shape the receptive fields of their efferent grcs. They could at most sharpen the response selectivity of grcs by setting their threshold as proposed by Marr (1969). We propose that, in addition, Gocs are involved in synchronization and rhythmogenesis.

Our study also suggests that PFs have a much more important function in regulating granular layer activity than generally is assumed. According to the present hypothesis, PFs synchronize Gocs over long distances. It is interesting to note that the present view on PFs goes opposite to the clock hypothesis of Braitenberg et al. (1997), according to whom the slow conduction speed of PFs is essential for the generation of the time delays that cause adjacent (Purkinje) cells to fire *asynchronously*.

Finally, with respect to the Purkinje cells, it has been suggested in previous modeling studies that they might be able to phase-lock their spike responses to PF inputs only when many PF synapses are activated synchronously (De Schutter 1994; De Schutter and Bower 1994b; Jaeger et al. 1997). Consequently, the synchronization of PF activity imposed by the Goc-grc feedback loop could provide a critical mechanism for the precise timing of Purkinje cell firing and could be important for plasticity of their PF synapses (De Schutter 1995; Hartell 1996).

APPENDIX

In this appendix we give a full description of the equations and parameters governing the network model.

$$I_{\text{applied}} = C\frac{dV}{dt} + \frac{1}{R}(V - V_{\text{leak}}) + \sum_{\text{channel}} g_{\text{channel}}(V - V_{\text{channel}}) + \sum_{\text{synapse}} g_{\text{synapse}}(V - V_{\text{synapse}})$$

The values of C and R (see METHODS) have been calculated from the surface area using a specific membrane capacitance of 1 μF/cm^2 and a specific membrane resistance of 30,300 Ωcm^2.

Equations for voltage-gated channels

$$g_{\text{channel}}(t,V) = \bar{g}m^p h$$

$$\frac{dm}{dt} = \alpha(1 - m) - \beta m, \quad \tau = \frac{1}{\alpha + \beta}, \quad m_\infty = \frac{\alpha}{\tau}$$

$$\text{Exponential (Exp):} \quad \alpha(V) = Ae^{B(V_m - V_0)} + C$$

$$\text{Sigmoid (Sig):} \quad \alpha(V) = \frac{A}{1 + e^{B(V_m - V_0)}}$$

$$\text{Linoid (Lin):} \quad \alpha(V) = \frac{A(V_m - V_0)}{e^{B(V_m - V_0)} - 1}$$

$$\text{KC}\alpha: \quad \alpha(V,[\text{Ca}^{2+}]_i) = \frac{A}{1 + \frac{Ce^{\text{BV}_m}}{[Ca^{2+}]_i}}$$

$$\text{KC}\beta: \quad \alpha(V,[\text{Ca}^{2+}]_i) = \frac{A}{1 + \frac{[Ca^{2+}]_i}{Ce^{\text{BV}_m}}}$$

The channels' parameter values are listed in Table 1. They have been adapted (see METHODS) from Gabbiani et al. (1994), except for the KA channel, which was adapted from Bardoni and Belluzzi (1993). In addition, for granule cells, all voltage-dependent functions have been shifted 10 mV toward more positive voltages, i.e., $V_m = V$ - 10 while $V_m = V$ for Gocs. For the peak conductance values $\bar{g}$, see METHODS.

Equations for synaptic receptor channels

Synaptic receptor conductances were modeled as dual exponential functions (Wilson and Bower 1989)

$$g_{\text{synapse}}(t,V) = \bar{g}\frac{(\tau_1 - \tau_2)(e^{-t/\tau_1} - e^{-t/\tau_2})}{\tau_1\tau_2(e^{-t_{\text{peak}}/\tau_1} - e^{-t_{\text{peak}}/\tau_2})}\frac{1}{1 + \eta[Mg^{2+}]e^{-\gamma V_m}}$$

$$\text{with } t_{\text{peak}} = \frac{\tau_1\tau_2\ln(\tau_1/\tau_2)}{\tau_1 - \tau_2} \text{ and } [\text{Mg}^{2+}] = 1.2 \text{ mM}$$

TABLE 1. *Parameter values of voltage-gated channels*

Channel	$V_{channel}$, mV	P				A, ms^{-1}	B, mV^{-1}	C, ms^{-1}	V_0, mV	Constraints
NaF	55	3	m	α	Exp	7.5	0.081		−39	
				β	Exp	7.5	−0.066		−39	$\tau > 0.01$ ms
			h	α	Exp	0.6	−0.089		−50	
				β	Exp	0.6	0.089		−50	$\tau > 0.045$ ms
Kdr	−90	4	m	α	Exp	0.85	0.073		−38	
				β	Exp	0.85	−0.018		−38	
			h	α	Exp	3e-4	−0.08	35e-4	−46	$\alpha > 38$e-4
				β	Sig	5.5e-3	−0.0807		−44	
CaL	80	2	m	α	Sig	8.0	−0.072		5	
				β	Lin	0.1	0.2		−8.9	
			h	α	Exp	0.025	−0.05		−60	$\alpha > 0.025$
				β	Exp	−0.025	−0.05	0.025	−60	$\beta > 0.0$
H	−42	1	m	α	Exp	4e-3	−0.0909		−75	
				β	Exp	4e-3	0.0909		−75	
KA	−90	3	m	τ	Exp	0.41	−1/42.8	0.167	−43.5	
				m_∞	Sig	1	−1/19.8		−46.7	
			h	τ	*					
				h_∞	Sig	1	1/8.4		−78.8	
KC	−90	1	m	α	KC α	12.5	−0.085	1.5e-3		
				β	KC β	7.5	−0.077	150e-6		

A and C values for KA are in ms for τ and dimensionless for m_∞ and h_∞; C values in KC are in mM. NaF, inactivating Na^+ channel; Kdr, delayed rectifier; CaL, high-voltage-activated Ca^{2+} channel; H, anomalous inward rectifier; KA, A-type K^+ channel; KC, Ca^{2+}-dependent K^+ channel. * $\tau(V) = 10.8 + 0.03V_m + 1/(57.9e^{0.127V_m} + 0.000134e^{-0.059V_m})$.

The value of η is zero except for NMDA-receptor channels ($\eta = 0.2801\ mM^{-1}$, $\gamma = 0.062\ mV^{-1}$). The reversal potentials $V_{synapse}$ are 0 mV (AMPA and NMDA) and −70 mV ($GABA_A$ channels). For the peak conductance values $\bar{g}$ and the time constants τ_1 and τ_2, see METHODS, *Granule cells*.

Equations for calcium pools

The neuronal calcium dynamics were reduced to that of a single exponentially decaying Ca^{2+} pool (De Schutter and Smolen 1998) with a resting concentration of 75.5 nM and a time constant of 10 ms (grcs) or 200 ms (Gocs).

$$\frac{d[Ca^{2+}]_i}{dt} = \frac{I_{CaL}}{2FAd} - \frac{[Ca^{2+}]_i - [Ca^{2+}]_{rest}}{\tau}, \text{ with } [Ca^{2+}]_{rest} = 75.5 \text{ nM}$$

F = 96,494 C/mol, τ = 10 ms (grcs) or 200 ms (Gocs), A = cell surface area, and d = thickness of the submembrane shell [0.084 μm (grcs) or 0.091 μm (Gocs)].

We thank S. Dieudonné for providing a preprint of his paper and B. Vos and S. Dieudonné for helpful discussions.

This work was supported by the Human Frontiers Science Program, Research Project G.0113.96 of the Fund for Scientific Research (Flanders), and by the University of Antwerp.

Address for reprint requests: R. Maex, Born-Bunge Foundation, University of Antwerp, Universiteitsplein 1, B-2610 Antwerp, Belgium.

E-mail: reinoud@bbf.uia.ac.be.

Received 29 December 1997; accepted in final form 10 August 1998.

REFERENCES

ALBUS, J. S. A theory of cerebellar function. *Math. Biosci.* 10: 25–61, 1971.

ARMSTRONG, D. M. AND RAWSON, J. A. Activity patterns of cerebellar cortical neurones and climbing fibre afferents in the awake cat. *J. Physiol. (Lond.)* 289: 425–448, 1979.

ATKINS, M. J., VAN ALPHEN, A. M., AND SIMPSON, J. I. Characteristics of putative Golgi cells in the rabbit cerebellar flocculus. *Soc. Neurosci. Abstr.* 23: 1287, 1997.

BARBOUR, B. Synaptic currents evoked in Purkinje cells by stimulating individual granule cells. *Neuron* 11: 759–769, 1993.

BARDONI, R. AND BELLUZZI, O. Kinetic study and numerical reconstruction of A-type current in granule cells of rat cerebellar slices. *J. Neurophysiol.* 69: 2222–2231, 1993.

BERNARD, C. AND AXELRAD, H. Propagation of parallel fiber volleys in the cerebellar cortex: a computer simulation. *Brain Res.* 565: 195–208, 1991.

BOWER, J. M. AND BEEMAN, D. *The Book of GENESIS: Exploring Realistic Neural Models with the GEneral NEural SImulation System*. New York: TELOS, 1995.

BOWER, J. M. AND KASSEL, J. Variability in tactile projection patterns to cerebellar folia crus IIA of the Norway rat. *J. Comp. Neurol.* 302: 768–778, 1990.

BRAITENBERG, V., HECK, D., AND SULTAN, F. The detection and generation of sequences as a key to cerebellar function. Experiments and theory. *Behav. Brain Sci.* 20: 229–245, 1997.

BRICKLEY, S. G., CULL-CANDY, S. G., AND FARRANT, M. Development of a tonic form of synaptic inhibition in rat cerebellar granule cells resulting from persistent activation of $GABA_A$ receptors. *J. Physiol. (Lond.)* 497: 753–759, 1996.

BRODAL, P. AND BJAALIE, J. G. Organization of the pontine nuclei. *Neurosci. Res.* 13: 83–118, 1992.

BRODAL, P. AND BJAALIE, J. G. Salient anatomic features of the cortico-ponto-cerebellar pathway. *Prog. Brain Res.* 114: 227–249, 1997.

BUSH, P. AND SEJNOWSKI, T. Inhibition synchronizes sparsely connected cortical neurons within and between columns in realistic network models. *J. Comput. Neurosci.* 3: 91–110, 1996.

CHAUVET, G. A. On associative motor learning by the cerebellar cortex: from Purkinje unit to network with variational learning rules. *Math. Biosci.* 126: 41–79, 1995.

COBB, S. R., BUHL, E. H., HALASY, K., PAULSEN, O., AND SOMOGYI, P. Synchronization of neuronal activity in hippocampus by individual GABAergic interneurons. *Nature* 378: 75–78, 1995.

CROOK, S. M., ERMENTROUT, G. B., VANIER, M. C., AND BOWER, J. M. The role of axonal delay in the synchronization of networks of coupled cortical oscillators. *J. Comput. Neurosci.* 4: 161–172, 1997.

CULL-CANDY, S. G., MARSHALL, C. G., AND OGDEN, D. Voltage-activated membrane currents in rat cerebellar granule neurones. *J. Physiol. (Lond.)* 414: 179–199, 1989.

D'ANGELO, E., DE FILIPPI, G., ROSSI, P., AND TAGLIETTI, V. Synaptic excitation of individual rat cerebellar granule cells in situ: evidence for the role of NMDA receptors. *J. Physiol. (Lond.)* 482: 397–413, 1995.

DE SCHUTTER, E. Modelling the cerebellar Purkinje cell: experiments in computo. *Prog. Brain Res.* 102: 427–441, 1994.

DE SCHUTTER, E. Cerebellar long-term depression might normalize excitation of Purkinje cells: a hypothesis. *Trends Neurosci.* 18: 291–295, 1995.

DE SCHUTTER, E. AND BOWER, J. M. An active membrane model of the cerebellar Purkinje cell. I. Simulation of current clamps in slice. *J. Neurophysiol.* 71: 375–400, 1994a.

DE SCHUTTER, E. AND BOWER, J. M. Simulated responses of cerebellar Purkinje cells are independent of the dendritic location of granule cell synaptic inputs. *Proc. Natl. Acad. Sci. USA* 91: 4736–4740, 1994b.

DE SCHUTTER, E. AND MAEX, R. The cerebellum: cortical processing and theory. *Curr. Opin. Neurobiol.* 6: 759–764, 1996.

DE SCHUTTER, E. AND SMOLEN, P. Calcium dynamics in large neuronal models. In: *Methods in Neuronal Modeling: From Synapses to Networks* (2nd ed.), edited by C. Koch and I. Segev. Cambridge, MA: MIT Press, 1998, p. 211–250.

DE ZEEUW, C. I., WYLIE, D. R., DIGIORGI, P. L., AND SIMPSON, J. I. Morphological evidence for interzonal inhibition by Golgi cells in the rabbit vestibulocerebellum. *Soc. Neurosci. Abstr.* 20: 1745, 1995.

DESTEXHE, A., BAL, T., MCCORMICK, D. A., AND SEJNOWSKI, T. J. Ionic mechanisms underlying synchronized oscillations and propagating waves in a model of ferret thalamic slices. *J. Neurophysiol.* 76: 2049–2070, 1996.

DIEUDONNÉ, S. Glycinergic synaptic currents in Golgi cells of the rat cerebellum. *Proc. Natl. Acad. Sci. USA* 92: 1441–1445, 1995.

DIEUDONNÉ, S. Submillisecond kinetics and low efficacy of parallel fibre-Golgi cell synaptic currents in the rat cerebellum. *J. Physiol. (Lond.)* 510: 845–866, 1998.

DIEUDONNÉ, S. AND KEHOE, J. S. Characterization of Golgi interneurons in the rat cerebellum. *Soc. Neurosci. Abstr.* 22: 1632, 1996.

ECCLES, J. C., FABER, D. S., MURPHY, J. T., SABAH, N. H., AND TÁBORÍKOVÁ, H. Afferent volleys in limb nerves influencing impulse discharges in cerebellar cortex. I. In mossy fibers and granule cells. *Exp. Brain Res.* 13: 15–35, 1971.

ECCLES, J. C., ITO, M., AND SZENTÁGOTHAI, J. *The Cerebellum as a Neuronal Machine*. Berlin: Springer-Verlag, 1967.

ECCLES, J. C., LLINÁS, R., AND SASAKI, K. Parallel fibre stimulation and the responses induced thereby in the Purkinje cells of the cerebellum. *Exp. Brain Res.* 1: 17–39, 1966.

EDGLEY, S. A. AND LIDIERTH, M. The discharges of cerebellar Golgi cells during locomotion in the cat. *J. Physiol. (Lond.)* 392: 315–332, 1987.

ERMENTROUT, G. B. AND KOPELL, N. Fine structure of neural spiking and synchronization in the presence of conduction delays. *Proc. Natl. Acad. Sci. USA* 95: 1259–1264, 1998.

FREEMAN, W. J. Waves, pulses, and the theory of neural masses. In: *Progress in Theoretical Biology*, edited by R. Rosen and F. M. Snell. New York: Academy Press, 1972, vol. 2, p. 87–165.

GABBIANI, F., MIDTGAARD, J., AND KNÖPFEL, T. Synaptic integration in a model of cerebellar granule cells. *J. Neurophysiol.* 72: 999–1009, 1994 (corrigenda February 1996).

GOLOMB, D. AND RINZEL, J. Dynamics of globally coupled inhibitory neurons with heterogeneity. *Phys. Rev. E* 48: 4810–4814, 1993.

HANSEL, D., MATO, G., AND MEUNIER, C. Synchrony in excitatory neural networks. *Neural Comput.* 7: 307–337, 1995.

HARTELL, N. A. Strong activation of parallel fibers produces localized calcium transients and a form of LTD that spreads to distant synapses. *Neuron* 16: 601–610, 1996.

HARTMANN, M. J. AND BOWER, J. M. Oscillatory activity in the cerebellar hemispheres of unrestrained rats. *J. Neurophysiol.* 80: 1598–1604, 1998.

HARVEY, R. J. AND NAPPER, R. M. A. Quantitative studies of the mammalian cerebellum. *Prog. Neurobiol.* 36: 437–463, 1991.

HILLE, B. *Ionic Channels of Excitable Membranes*. Sunderland, MA: Sinauer, 1992.

ITO, M. *The Cerebellum and Neural Control*. New York: Raven Press, 1984.

JAEGER, D., DE SCHUTTER, E., AND BOWER, J. M. The role of synaptic and voltage-gated currents in the control of Purkinje cell spiking: a modeling study. *J. Neurosci.* 17: 91–106, 1997.

JAKAB, R. L. AND HÁMORI, J. Quantitative morphology and synaptology of cerebellar glomeruli in the rat. *Anat. Embryol.* 179: 81–88, 1988.

JEFFERYS, J.G.R., TRAUB, R. D., AND WHITTINGTON, M. A. Neuronal networks for induced '40 Hz' rhythms. *Trends Neurosci.* 19: 202–208, 1996.

KAMMEN, D. M., HOLMES, P. J., AND KOCH, C. Cortical architecture and oscillations in neuronal networks: feedback versus local coupling. In: *Models of Brain Function*, edited by R.M.J. Cotterill. Cambridge, UK: Cambridge Univ. Press, 1989, p. 273–284.

KANEDA, M., FARRANT, M., AND CULL-CANDY, S. G. Whole-cell and single-channel currents activated by GABA and glycine in granule cells of the rat cerebellum. *J. Physiol. (Lond.)* 485: 419–435, 1995.

LYTTON, W. W. AND SEJNOWSKI, T. J. Simulations of cortical pyramidal neurons synchronized by inhibitory interneurons. *J. Neurophysiol.* 66: 1059–1079, 1991.

MAEX, R. AND DE SCHUTTER, E. The critical synaptic number for rhythmogenesis and synchronization in a network model of the cerebellar granular layer. In: *ICANN 98 Proceedings of the 8th International Conference on Artificial Neural Networks in Skövde, Sweden*, edited by L. Niklasson, M. Bodén, and T. Ziemke. London: Springer-Verlag, 1998, p. 361–366.

MAEX, R. AND ORBAN, G. A. Model circuit of spiking neurons generating directional selectivity in simple cells. *J. Neurophysiol.* 75: 1515–1545, 1996.

MAEX, R., VOS, B. P., AND DE SCHUTTER, E. Dynamics of a detailed model of the granular layer of the cerebellum. *Soc. Neurosci. Abstr.* 22: 1093, 1996.

MANOR, Y., RINZEL, J., SEGEV, I., AND YAROM, Y. Low-amplitude oscillations in the inferior olive: a model based on electrical coupling of neurons with heterogeneous channel densities. *J. Neurophysiol.* 77: 2736–2752, 1997.

MARR, D. A theory of cerebellar cortex. *J. Physiol. (Lond.)* 202: 437–470, 1969.

MIDTGAARD, J. Membrane properties and synaptic responses of Golgi cells and stellate cells in the turtle cerebellum in vitro. *J. Physiol. (Lond.)* 457: 329–354, 1992.

MILES, F. A., FULLER, J. H., BRAITMAN, D. J., AND DOW, B. M. Long-term adaptive changes in primate vestibuloocular reflex. III. Electrophysiological observations in flocculus of normal monkeys. *J. Neurophysiol.* 43: 1437–1476, 1980.

MOORE, J. W., DESMOND, J. E., AND BERTHIER, N. E. Adaptively timed conditioned responses and the cerebellum: a neural network approach. *Biol. Cybern.* 62: 17–28, 1989.

MUGNAINI, E. The length of cerebellar parallel fibers in chicken and rhesus monkey. *J. Comp. Neurol.* 220: 7–15, 1983.

NUSSER, Z., ROBERTS, J. D. B., BAUDE, A., RICHARDS, J. G., AND SOMOGYI, P. Relative densities of synaptic and extrasynaptic $GABA_A$ receptors on cerebellar granule cells as determined by a quantitative immunogold method. *J. Neurosci.* 15: 2948–2960, 1995.

OTIS, T. S. AND MODY, I. Modulation of decay kinetics and frequency of $GABA_A$ receptor-mediated spontaneous inhibitory postsynaptic currents in hippocampal neurons. *Neuroscience* 49: 13–32, 1992.

PALAY, S. L. AND CHAN-PALAY, V. *Cerebellar Cortex*. New York: Springer-Verlag, 1974.

PALKOVITS, M., MAGYAR, P., AND SZENTÁGOTHAI, J. Quantitative histological analysis of the cerebellar cortex in the cat. II. Cell numbers and densities in the granular layer. *Brain Res.* 32: 15–30, 1971.

PELLERIN, J.-P. AND LAMARRE, Y. Local field potential oscillations in primate cerebellar cortex during voluntary movement. *J. Neurophysiol.* 78: 3502–3507, 1997.

PELLIONISZ, A. AND SZENTÁGOTHAI, J. Dynamic single unit simulation of a realistic cerebellar network model. *Brain Res.* 49: 83–99, 1973.

PICHITPORNCHAI, C., RAWSON, J. A., AND REES, S. Morphology of parallel fibres in the cerebellar cortex of the rat: an experimental light and electron microscopic study with biocytin. *J. Comp. Neurol.* 342: 206–220, 1994.

PUIA, G., COSTA, E., AND VICINI, S. Functional diversity of GABA-activated Cl^- currents in Purkinje versus granule neurons in rat cerebellar slices. *Neuron* 12: 117–126, 1994.

RINZEL, J. AND ERMENTROUT, G. B. Analysis of neural excitability and oscillations. In: *Methods in Neuronal Modeling: From Synapses to Networks*, edited by C. Koch and I. Segev. Cambridge, MA: MIT Press, 1989, p. 135–169.

SCHILLEN, T. B. AND KÖNIG, P. Stimulus-dependent assembly formation of oscillatory responses. II. Desynchronization. *Neural Comput.* 3: 167–178, 1991.

SHAMBES, G. M., GIBSON, J. M., AND WELKER, W. Fractured somatotopy in granule cell tactile areas of rat cerebellar hemispheres revealed by micromapping. *Brain Behav. Evol.* 15: 94–140, 1978.

SILVER, R. A., COLQUHOUN, D., CULL-CANDY, S. G., AND EDMONDS, B. Deactivation and desensitization of non-NMDA receptors in patches and the time course of EPSCs in rat cerebellar granule cells. *J. Physiol. (Lond.)* 493: 167–173, 1996.

SILVER, R. A., TRAYNELIS, S. F., AND CULL-CANDY, S. G. Rapid-time-course miniature and evoked excitatory currents at cerebellar synapses in situ. *Nature* 355: 163–166, 1992.

TRAUB, R. D., JEFFERYS, J.G.R., AND WHITTINGTON, M. A. Simulation of gamma rhythms in networks of interneurons and pyramidal cells. *J. Comput. Neurosci.* 4: 141–150, 1997.

TRAUB, R. D., WHITTINGTON, M. A., STANFORD, I. M., AND JEFFERYS, J. G. R. A mechanism for generation of long-range synchronous fast oscillations in the cortex. *Nature* 383: 621–624, 1996.

TURRIGIANO, G. G., LESLIE, K. R., DESAI, N. S., RUTHERFORD, L. C., AND NELSON, S. B. Activity-dependent scaling of quantal amplitude in neocortical neurons. *Nature* 391: 892–896, 1998.

VAN KAN, P.L.E., GIBSON, A. R., AND HOUK, J. C. Movement-related inputs to intermediate cerebellum of the monkey. *J. Neurophysiol.* 69: 74–94, 1993.

VOS, B. P., MAEX, R., AND DE SCHUTTER, E. Correlation of firing between rat cerebellar Golgi cells. *Soc. Neurosci. Abstr.* 23: 1286, 1997.

VRANESIC, I., IIJIMA, T., ICHIKAWA, M., MATSUMOTO, G., AND KNÖPFEL, T. Signal transmission in the parallel fiber-Purkinje cell system visualized by high-resolution imaging. *Proc. Natl. Acad. Sci. USA* 91: 13014–13017, 1994.

WALL, M. J. AND USOWICZ, M. M. Development of action potential-dependent and independent spontaneous $GABA_A$ receptor-mediated currents in granule cells of postnatal rat cerebellum. *Eur. J. Neurosci.* 9: 533–548, 1997.

WANG, X.-J. AND BUZSÁKI, G. Gamma oscillation by synaptic inhibition in a hippocampal interneuronal network model. *J. Neurosci.* 16: 6402–6413, 1996.

WHITTINGTON, M. A., TRAUB, R. D., AND JEFFERYS, J.G.R. Synchronized oscillations in interneuron networks driven by metabotropic glutamate receptor activation. *Nature* 373: 612–615, 1995.

WILSON, M. A. AND BOWER, J. M. The simulation of large-scale neural networks. In: *Methods in Neuronal Modeling: From Synapses to Networks*, edited by C. Koch and I. Segev. Cambridge, MA: MIT Press, 1989, p. 291–333.